Chlorophyll-a algorithms for oligotrophic oceans: A novel approach based on three-band reflectance difference

Chuanmin Hu[1], Zhongping Lee[2], Bryan Franz[3]
[1]University of South Florida; [2]Mississippi State University; [3]NASA GSFC
Email: hu@marine.usf.edu

Abstract

A new empirical algorithm is proposed to estimate surface chlorophyll-a concentrations (Chl) in the global ocean for Chl ≤ 0.25 mg m^{-3} (~ 77% of the global ocean area). The algorithm is based on a color index (CI), defined as the difference between remote sensing reflectance (R_{rs}, sr^{-1}) in the green and a reference formed linearly between R_{rs} in the blue and red. For low Chl waters, *in situ* data showed a tighter (and therefore better) relationship between CI and Chl than between traditional band-ratios and Chl, which was further validated using global data collected concurrently by ship-borne and SeaWiFS satellite instruments. Model simulations showed that for low Chl waters, compared with the band-ratio algorithm, the CI-based algorithm (CIA) was more tolerant to changes in chlorophyll-specific backscattering coefficient, and performed similarly for different relative contributions of non-phytoplankton absorption. Simulations using existing atmospheric correction approaches further demonstrated that the CIA was much less sensitive than band-ratio algorithms to various errors induced by instrument noise and imperfect atmospheric correction (including sun glint and whitecap corrections). Image and time-series analyses of SeaWiFS and MODIS/Aqua data also showed improved performance in terms of reduced image noise, more coherent spatial and temporal patterns, and consistency between the two sensors. The reduction in noise and other errors is particularly useful to improve the detection of various ocean features such as eddies. Preliminary tests over MERIS and CZCS data indicate that the new approach should be generally applicable to all existing and future ocean color instruments.

Keywords: Remote sensing, ocean color, SeaWiFS, MODIS, MERIS, CZCS, bio-optical inversion, atmospheric correction, chlorophyll-a, calibration, validation, climate data record.

1. Introduction

Over the past half century, algorithms to invert ocean color (i.e., spectral radiance or reflectance of the surface ocean) to phytoplankton chlorophyll-a concentrations (Chl in mg m^{-3}) have evolved from simple empirical regressions [Gordon and Morel, 1983] to semi-analytical inversions based on radiative transfer theory [Sathyendranath et al., 1989; Carder et al., 1999; Maritorena et al., 2002; others]. While each of these has its own advantages and disadvantages (and thus, applicability range), an algorithm based on a spectral ratio of remote-sensing reflectance (R_{rs}, sr^{-1}) has historically been used as the default algorithm formulation to produce global chlorophyll-a products from measurements made by satellite instruments. These include the Coastal Zone Color Scanner (CZCS, 1978-1986), the Sea-viewing Wide Field-of-view Sensor (SeaWiFS, 1997-2010) and the Moderate Resolution Imaging Spectroradiometer (MODIS, 1999 – present for Terra satellite and 2002 – present for Aqua satellite). The current default Chl algorithm for SeaWiFS and MODIS is based on the OCx form of O'Reilly et al. (2000), with coefficients derived using *in situ* data from the NASA bio-Optical Marine Algorithm Dataset (NOMAD) version 2 [http://oceancolor.gsfc.nasa.gov/REPROCESSING/R2009/ocv6/]. The default SeaWiFS algorithm is referred to as OC4 in this paper. Correspondingly, many large-scale studies of ocean carbon cycles and biogeochemistry that utilized satellite ocean color data, from regional-, basin-, to global-scale, have used the OC4 data products [e.g., Gregg et al., 2005; Behrenfeld et al., 2006; Yoder and Kennelly, 2006; Polovina et al., 2008], leading to documented changes in Chl_{OC4} and primary productivity at various spatial/temporal scales and connections to climate variability.

An early review on the history of the band-ratio empirical algorithms as well as their advantages and disadvantages was provided in Gordon and Morel [1983], and recently re-visited by Dierssen [2010]. Briefly, the most recent OC4v6 algorithm evolved from its predecessors in the 1970s and 1980s [Clarke et al., 1970; Arvesen et al., 1973; Hovis and Leung, 1977, Clark et al., 1980; Gordon and Clark, 1980; Morel, 1980], when the radiance ratio of blue and green wavelengths was recognized to correlate well with surface Chl. The underlying assumption is that the relative changes between the blue and green bands are primarily driven by changes in phytoplankton and their direct degradation products (i.e., the traditional Case-I scenario, see Morel and Prieur, 1977), and the latter can therefore be inferred from the former. Indeed, despite the various studies showing the algorithm artifacts in non-Case-I (i.e., Case-II) waters [e.g., Dierssen et al., 2002; Hu et al., 2003; Odriozola et al., 2007; others], global validation efforts of the SeaWiFS Chl_{OC4} data products proved that for most open ocean waters, the algorithm performed well, with RMS differences from ship-based Chl (after logarithmic transformation) of 0.2 – 0.3 without significant bias [Gregg and Casey, 2004; McClain et al., 2004; McClain, 2009]. Agreement/disagreement varied among different ocean basins because the same regression coefficients, determined from the global dataset optimization, were applied universally [Gregg and Casey, 2004]. To address these regional differences, various band combinations and regression coefficients were developed for different water types [e.g., Kahru and Mitchell, 1999; McKee et al., 2007; Mitchell and Kahru, 2009], with similar band-ratio forms.

All previous global-scale studies used spatially and temporally composited data (e.g., monthly composites at reduced resolution) to reduce data volume and fill in data gaps due to cloud cover and other measurement/algorithm artifacts. Chl data product errors at original spatial and temporal resolutions are smoothed and smeared in these higher-level data products, thus complicating the propagation of errors to trend/variability analyses at global or regional scales. These errors are particularly evident at low concentrations (Chl < 0.1 mg m^3). Fig. 1a shows a typical example of SeaWiFS Global Area Coverage (GAC) Level-2 Chl data product for the Sargasso Sea, an oligotrophic ocean gyre in the North Atlantic. Due to a variety of reasons (see details below), the image shows patchiness, speckle noise (pixelization), and is not spatially coherent. Note that all non-zero Chl values in this image are regarded as acceptable-quality and used in composing the higher-level (i.e., lower spatial and temporal resolution) products, because all "low-quality" data, as defined by the various quality flags, are already discarded. The image was selected rather arbitrarily for demonstration purpose, and similar problems could be visualized in almost every Level-2 GAC image. Clearly, these issues need to be addressed in order to understand how they may propagate to higher-level products to affect the large-scale trend/variability analyses.

Recently, to derive spatially coherent and temporally consistent ocean color patterns from satellite images contaminated by severe sun glint, a new color index (CI) was developed for satellite ocean color observations ([Hu, 2011]. Instead of using a blue-green band-ratio as the independent variable, the CI is calculated as the difference between the green-band reflectance and a reference formed linearly by the blue and red bands. This is similar to the design of the MODIS fluorescence line height (FLH, Letelier and Abott, 1996) and MERIS maximal chlorophyll index (MCI, Gower et al., 2005), except that the bands are shifted to blue-green-red. Hu [2009] used a similar form to detect and quantify the reflectance peak in the MODIS 859-nm band, and proved that the floating algae index (FAI), derived using the 645-859-1240 band combination, was much less sensitive to variable observing conditions (aerosols, sun glint, thin clouds, solar/viewing geometry) than band-ratio algorithms. The MODIS CI appears to be relatively insensitive to residual errors due to imperfect empirical glint correction, and in glint-free areas it is also well correlated with MODIS band-ratio Chl [Hu, 2011], suggesting that a new Chl algorithm might be developed to remove residual atmosphere-correction related errors and image noise.

Inspired by these recent works, a new empirical algorithm to retrieve Chl using the CI as the independent variable is developed and validated in this paper. Using data collected primarily by SeaWiFS but also by MODIS/Aqua and other satellite instruments, we evaluate the performance of such a band-difference algorithm (i.e., the CI algorithm or CIA) in comparison with the OC4 band-ratio algorithm. We demonstrate and argue that because the CI is much more tolerant than the band ratio to various perturbations in sensor hardware and data processing (e.g., instrument noise, residual errors in atmospheric correction, whitecap and sun glint corrections, stray light contamination), and also more tolerant to perturbations of Chl-independent particle backscattering from the water column, the CIA appears superior to band-ratio algorithms in deriving a more consistent and accurate Chl climate data record for most oligotrophic oceans.

The paper is arranged as follows. The principles to "measure" Chl from space, although found in the refereed literature, are briefly introduced for the reader's convenience. The *in situ* and satellite data used to develop and validate the new algorithm are then described. Following that, the new Chl algorithm (CIA) is described and validated for SeaWiFS. Its sensitivity to errors and perturbations, in comparison with the OC4 algorithm, is analyzed in detail, and further demonstrated using satellite measurements. Sample time-series at several arbitrarily selected oligotrohpic ocean sites as well as from global-scale data are used to evaluate the performance of the new algorithm. Finally, we discuss the new algorithm's applicability to other satellite instruments such as MODIS, MERIS, and CZCS, and discuss its potential to improve data quality, time-series and cross-sensor consistency, and to improve image quality in feature detection.

2. Principles to "measure" Chl from space

A multi-band ocean-color satellite instrument measures the top-of-atmosphere (TOA) radiance or reflectance in several spectral bands coving the visible to the near-infrared domain. On SeaWiFS, the spectral bands are centered at λ=412, 443, 490, 510, 555, 670, 765, and 865 nm, respectively. After radiometric calibration (including in-orbit vicarious calibration, Franz et al., 2007) the calibrated at-sensor reflectance ($\rho_t(\lambda)$) is used to derive the at-sea remote sensing reflectance (R_{rs}) [Gordon, 1997]. With some simplifications, this can be expressed as:

$$\rho_t(\lambda) = \rho_r(\lambda) + \rho_{ar}(\lambda) + t(\lambda)\rho_{wc}(\lambda)+T(\lambda)\rho_g(\lambda) + \pi t(\lambda)t_0(\lambda)R_{rs}(\lambda), \qquad (1)$$

where ρ_r is that due to Rayleigh scattering, ρ_{ar} is that due to aerosol scattering and aerosol-Rayleigh interactions, ρ_{wc} is the whitecap reflectance, ρ_g is the sun glint reflectance, T and t are the direct and diffuse transmittance from the target (pixel of the imagery) to the sensor (satellite), and t_0 is the diffuse transmittance from the sun to the target.

Deriving $R_{rs}(\lambda)$ from $\rho_t(\lambda)$ is through a sophisticated atmospheric correction, which uses lookup tables for aerosol and molecular properties [Gordon and Wang, 1994a&b, Ahmad et al., 2010, Bailey et al., 2010] after removing contributions from whitecaps [Frouin et al. 1996] and sun glint [Wang and Bailey, 2001]. The retrieved $R_{rs}(\lambda)$ is then used as the input to an established bio-optical inversion model to derive Chl. For the OC4 algorithm, Chl is derived as [O'Reilly et al., 2000]:

$$\mathrm{Chl}_{OC4} = 10^{a0 + a1*\chi + a2*\chi*\chi + a3*\chi*\chi*\chi + a4*\chi*\chi*\chi*\chi}$$

$$\chi = \log_{10}(R) \text{ and } R = \max(R_{rs}(443, 490, 510))/R_{rs}(555), \qquad (2)$$

where a0 – a4 are the empirical regression coefficients, for which the current values (version 6) are 0.3272, -2.9940, 2.7218, -1.2259, -0.5683, respectively.

The algorithm details and their performance at global and regional scales can be found in the published literature as well as in online documents (http://oceancolor.gsfc.nasa.gov/REPROCESSING/R2009/ocv6/).

3. Data sources used in this study

In situ data were obtained from the NASA SeaBASS archive (SeaWiFS Bio-optical Archive and Storage System), which is a database of measurements collected by many research groups in order to develop and validate satellite ocean color algorithms. The NOMAD dataset, described by Werdell and Bailey [2005], is a subset of SeaBASS specifically compiled for bio-optical algorithm development, as it contains coincident measurements of Chl, $R_{rs}(\lambda)$, and other data collected simultaneously in the global oceans.

Like the current OC4 algorithm, the dataset used to develop the CIA was taken from NOMAD version 2, covering a period of 1991-2007 and containing 4459 data records. Similar to Morel et al. [2007a], the NOMAD data used in the present study for algorithm development are those with Chl determined via HPLC, since Chl determined from traditional fluorometric methods often suffer from contaminations by chlorophyll-*b* and chlorophyll-*c*, as demonstrated from data collected in the southern ocean [Marrari et al., 2006; Dierssen, 2010]. Further, we applied the following criteria to select data for the oligotrophic oceans: $R_{rs}(\lambda) > 0.0$ sr^{-1}, Chl > 0.0 mg m^{-3}, bottom depth > 30.0 m, and latitude between 60^{o}N and 60^{o}W. A total of 136 data records were obtained.

To evaluate the algorithm performance when applied to satellite data, *in situ* data were also obtained from the SeaBASS archive through online query. The following criteria were used to search for the *in situ* – satellite matching pairs: bottom depth > 30 m; solar zenith angle < 70^{o}; satellite zenith angle < 56^{o}, time difference between satellite and *in situ* measurements < 3 hours; satellite Chl variance (standard deviation divided by mean) from the 3x3 pixels centered at the *in situ* stations < 15%; difference between modeled and measured surface irradiance < 100%; wind speed < 35 m s^{-1}. For SeaWiFS, a total of 1424 matching pairs were obtained for 1998-2010.

The online query also resulted in the satellite Level-2 computer filenames corresponding to the matching pairs. These Level-2 data products were derived by the NASA Ocean Biology Processing Group (OBPG) using the most recent updates in algorithms and instrument calibration (Reprocessing 2010.0, SeaDAS6.1). The data products include Chl_{OC4}, aerosol optical thickness at 865 nm (τ_865), and $R_{rs}(\lambda)$. $R_{rs}(\lambda)$ data extracted from the Level-2 files were used as the input to derive Chl_{CI} (Chl from the CI algorithm) and compared with those determined from the *in situ* measurements.

To evaluate algorithm performance in constructing time series, SeaWiFS Level-2 data between 1998 and 2010 covering two oligotrophic gyres, namely in the Sargasso Sea (15 to 35^{o}N, 60 – 40^{o}W) and in the eastern South Pacific Gyre (20 to 40^{o}S, 120 to 100^{o}W), were obtained from the

NASA GSFC. For cross-sensor consistency evaluations, SeaWiFS and MODIS/Aqua Level-2 global daily data for 2006 were used. Some Level-2 data files from MODIS/Aqua, MERIS, and CZCS covering the western North Atlantic Sea were also used for algorithm evaluation.

4. The new empirical Chl algorithm

Similar to the MODIS CI from the Rayleigh-corrected reflectance [Hu, 2011], the R_{rs}-based SeaWiFS CI is defined as the relative height of $R_{rs}(555)$ from a background, i.e., difference between $R_{rs}(555)$ and a baseline formed linearly between $R_{rs}(443)$ and $R_{rs}(670)$ (Fig. 2):

$$CI = R_{rs}(555) – [R_{rs}(443) + (555-443)/(670-443)*(R_{rs}(670)-R_{rs}(443))], \qquad (3)$$

which is approximately $CI \approx R_{rs}(555) – 0.5(R_{rs}(443) + R_{rs}(670))$.

By this definition, for most clear ocean waters CI is negative. Because for most clear waters $R_{rs}(670)$ is negligible (see the "clear water" concept in Gordon and Clark, 1981 and revisited in Morel and Maritorena, 2001), CI is basically a weighted relative difference between $R_{rs}(443)$ and $R_{rs}(555)$. Just as a ratio between the two is related to Chl, since $R_{rs}(555)$ is relatively stable but $R_{rs}(443)$ is sensitive to Chl changes for clear waters [Gordon and Morel, 1983], a difference between the two should also be related to Chl, and this forms the basis of the new Chl algorithm (the theoretical basis of this algorithm is provided in Section 6.1 below). Indeed, Fig. 2 shows that with increasing Chl, the magnitude of CI decreases monotonically. The added band at 670-nm has a great advantage in compensating various errors in atmospheric correction and other corrections when the algorithm is applied to satellite data (see below).

Using the NOMAD dataset, the relationships between band-ratio R and Chl (Eq. 2) and between CI and Chl are shown in Figs. 3a and 3b, respectively, for data collected from the 136 qualified stations. Also overlaid on Fig. 3a is the OC4v6 prediction (solid line), which shows that the globally optimized regression relationship fits well with the low Chl values. If a similar band-ratio form is developed using the low-concentration stations only (green dots), slightly better performance can be achieved as measured by the statistics (Table 1), but at the price of sacrificing the intermediate values (red line in Fig. 3a) because the numerical fit tends to plateau for Chl around 0.2 and 0.3 mg m^{-3}.

The statistical measure of the algorithm performance is listed in Table 1. Note that when evaluating the relative difference between the two datasets x and y (in this case, one is the *in situ* measurement (x) and the other is the algorithm prediction (y)), RMS difference (or error) is typically evaluated using the form of (y-x)/x. However, when one dataset contains substantial errors, the (y-x)/x ratio may be extremely large and therefore create biased estimates for the relative difference. For this reason, an "unbiased" RMS was also estimated using the form of (y-x)/(0.5x + 0.5y). And this evaluation was also used for comparison between satellite and *in situ* Chl data below. When the Chl data cover a large dynamic range they tend to be log-normal [Campbell, 1995]. Thus, R^2 between the log-transformed data was also estimated and presented in Table 1.

Fig. 3b shows that for low Chl values there is a strong relationship between CI and Chl, confirming the visual interpretation of Fig. 2. Non-linear regression for CI ≤ -0.0005 resulted in a coefficient of determination (R^2) of 0.95 (N=50) and a RMS difference of 16.52% between the CI-predicted Chl (Chl_{CI}) and the measured Chl:

$$Chl_{CI} = 10^{-0.4909 + 191.6590 * CI} \quad [CI \leq -0.0005 \ sr^{-1}] \qquad (4)$$

In comparison, for the same data points corresponding to CI ≤ -0.0005 sr^{-1} (N=50), the OC4v6 predicated Chl showed a lower coefficient of determination (R^2 = 0.85, N=50) and higher RMS difference from the *in situ* Chl (RMS = 34.87%). Even when new coefficients from these low-Chl data points were tuned to result in a better fit between band-ratio R and Chl, RMS difference was reduced to 22.95% but still higher than the CI predictions (Table 1). Indeed, the contrast between the different data scattering in Fig. 3a for Chl_{OC4} and Fig. 3b for Chl_{CI} is apparent. From this regression alone, the CIA appears to perform better than the OC4v6 for low concentrations (Chl ≤ 0.25 mg m^{-3}). Note that although the number of data points used in the regression is limited (N=50), they were collected from different ocean basins (Fig. 3a inset) covering the Pacific, Atlantic, Gulf of Mexico, and the Southern Ocean. Thus, the CIA might be applicable for most oligotrophic waters.

Fig. 3b also shows that the CIA may only be applicable for low concentrations, because the relationship quickly falls apart for CI > 0.0005 sr^{-1}, corresponding to Chl_{CI} ~ 0.4 mg m^{-3}. The reason why the CIA does not work well above this concentration is demonstrated in Sections 6.1 and 6.2 using radiative transfer modeling. Indeed, above this concentration, the CIA tends to underestimate Chl significantly (Fig. 3b), where the original OC4v6 should be used instead. For intermediate concentrations a mixture between the two algorithms may be used to assure image smoothness when the algorithm switches from one to another. For this practical consideration, the new global product of chlorophyll (Chl_{OCI}) is defined as follows:

$$
Chl_{OCI} = \begin{cases} Chl_{CI} & [\text{for } Chl_{CI} \leq 0.25 \text{ mg m}^{-3}] \\ Chl_{OC4} & [\text{for } Chl_{CI} > 0.4 \text{ mg m}^{-3}] \\ \alpha \times Chl_{OC4} + \beta \times Chl_{CI} & [\text{for } 0.25 < Chl_{CI} \leq 0.4 \text{ mg m}^{-3}], \end{cases} \quad (5)
$$

where $\alpha = (Chl_{CI} - 0.25)/(0.4 - 0.25)$, $\beta = (0.4 - Chl_{CI})/(0.4 - 0.25)$. Because such-derived Chl is from two algorithms (OC4 and CIA), we use the term Chl_{OCI} hereafter to represent the merged product.

5. Validation of the new Chl algorithm

The CIA was implemented to derive Chl_{OCI} from SeaWiFS Level-2 $R_{rs}(\lambda)$ data where concurrent *in situ* Chl were found (see data source). Fig. 4 shows the comparison between *in situ* Chl and satellite Chl_{OCI}, and between *in situ* Chl and satellite Chl_{OC4}. For high concentrations ($Chl_{OCI} >$ 0.4 mg m^{-3}) the data points between the two algorithms were forced to be identical (Eq. 5). For low concentrations (Chl $\leq$ 0.25 mg m^{-3}), the CI algorithm outperforms the OC4 algorithm by all measures, from RMS difference, R^2, to mean and median ratios (Table 2). Note that although only a limited number of data points were available for low concentrations, a slight improvement in algorithm performance may lead to larger difference in image analysis, because the majority of the ocean is oligotrophic. Indeed, analysis of the 13-year SeaWiFS monthly data between 1998 and 2010 indicated that 77.8±1.0% of the global ocean waters had surface Chl ≤ 0.25 mg m^{-3}, and 88.4±1.4% had surface Chl ≤ 0.4 mg m^{-3}. Thus, such a new algorithm might have profound effects on global-scale studies. Note that if a local OCx algorithm is developed for low concentrations only (Fig. 3a red line), its performance will also improve over the globally tuned OC4 algorithm in statistical measures and is also slightly better than the CIA in terms of median ratio. However, its R^2 value is lower than the CIA, especially when a linear form is used. Global validation results using this local OCx algorithm showed plateaued performance around 0.2-0.3 mg m^{-3}. More importantly, because it takes a similar band-ratio form, it suffers from same problems as encountered by the OC4 algorithm for low concentrations (see below). Thus, it is listed in the table for demonstration only and was not implemented for global data processing.

Because only limited *in situ* data are available to evaluate algorithm performance at low concentrations (e.g., there is no *in situ* Chl < 0.02 mg m^{-3}), below we take a theoretical approach to compare the sensitivity of $\mathrm{Chl_{CI}}$ and $\mathrm{Chl_{OC4}}$ algorithms to various perturbations, including sensor noise, atmospheric correction, and non-covarying in-water constituents.

6. Algorithm theoretical basis, and its sensitivity to simulated and realistic perturbations.

6.1. Algorithm theoretical basis: why and when it works

Assuming that the influence of measurement geometry (i.e., bi-directional reflectance effects) on $R_{rs}(\lambda)$ can be corrected [Morel and Gentili, 1993; Lee et al., 2011], $R_{rs}(\lambda)$ is entirely determined by the inherent optical properties (IOPs) through primarily spectral absorption and backscattering by the various in-water optically active constituents (OACs). These include water molecules, phytoplankton, colored dissolved organic matter (CDOM or yellow substance), and detrital particles. In high-wind seas, the OACs may also include bubbles induced by wave breaking, which may increase the backscattering properties significantly. Following Lee et al. [2010], $R_{rs}(\lambda)$ can be expressed using spectral absorption (a) and backscattering (b_b) coefficients as:

$$R_{\mathrm{rs}}(\lambda,\Omega) = \left(G_0^w(\Omega) + G_1^w(\Omega)\frac{b_{\mathrm{bw}}(\lambda)}{\kappa(\lambda)} \right)\frac{b_{\mathrm{bw}}(\lambda)}{\kappa(\lambda)} + \left(G_0^p(\Omega) + G_1^p(\Omega)\frac{b_{\mathrm{bp}}(\lambda)}{\kappa(\lambda)} \right)\frac{b_{\mathrm{bp}}(\lambda)}{\kappa(\lambda)}, \tag{6}$$

where the phase-function effects of molecular and particulate scatterings are separated explicitly. In Eq. (6), $\kappa = a + b_{\mathrm{b}}$, while Ω represents the solar/viewing geometry. A simplified form has often been used in the literature:

$$R_{rs}(\lambda) = G\frac{b_{bw}(\lambda) + b_{bp}(\lambda)}{a(\lambda)}, \tag{7}$$

where b_{bw} and b_{bp} are backscattering coefficients of water molecules (constant) and particles (variable), respectively.

Because $R_{\mathrm{rs}}(670)$ is generally negligible for oligotrophic waters, CI from Eq. 3 can be approximated as

$$CI \approx G\frac{(2a(443)\,b_{bw}(555) - a(555)\,b_{bw}(443)) + (2a(443)\,b_{bp}(555) - a(555)\,b_{bp}(443))}{2a(443)\,a(555)} \tag{8}$$

Because $b_{bw}(443) \approx 2.6\ b_{bw}(555)$, and $b_{bp}(443) \approx 1.6\ b_{bp}(555)$ (assuming a spectral slope of 2), Eq. 8 can be further simplified as

$$CI \approx -G\frac{(a(555)-0.8a(443))\,b_{bw}(443)+(a(555)-1.3a(443))\,b_{bp}(443)}{2a(443)\,a(555)} = -G\frac{\Delta_{water}+\Delta_{particles}}{2a(443)\,a(555)} \quad (9)$$

Fig. 5 shows the two backscattering related terms (Δ_{water} and $\Delta_{particles}$, x1000) for Chl ranging between 0.02 and 1.0 mg m^{-3}, estimated from the Morel and Moretorina [2001] Case-1 model. It shows that for Chl < ~0.4 mg m^{-3}, $|\Delta_{water}|$ overweighs $|\Delta_{particles}|$. This is due to two reasons: 1) low $b_{bp}(443)$ relative to $b_{bw}(443)$ (e.g., for Chl = 0.1 mg m^{-3}, $b_{bw}(443)$ = 0.0025 m^{-1}, $b_{bp}(443)$ ~0.0015 m^{-1}); 2) When Chl increases, the corresponding increase in $b_{bp}(443)$ is compensated by the decrease in (a(555)-1.3 a(443)). These results suggest that for Chl < 0.4 mg m^{-3}, Eq. 9 can be further simplified to

$$CI \propto -G\frac{b_{bw}(443)}{2a(443)}, \quad (10)$$

which is equivalent to the band ratio:

$$R = \frac{R_{rs}(443)}{R_{rs}(555)} \approx \frac{b_{bw}(443)+b_{bp}(443)}{b_{bw}(555)+b_{bp}(555)}\frac{a(555)}{a(443)} \quad (11)$$

In other words, both CI and R are inversely related to a(443). Because for oligotrophic waters a(443) is primarily a function of Chl, CI in Eq. 10 can be expressed as

$$CI \propto -G\frac{b_{bw}(443)}{2f(Chl)} \quad (12)$$

This simplified equation explains why Chl can be derived from CI at low concentrations.

6.2. Sensitivity to perturbations from in-water constituents

The empirical Chl algorithms (either OC4 or CIA) are based on the assumption that $R_{rs}(\lambda)$ is mainly determined by phytoplankton and its direct degradation product (the so called 'Case I' waters, Morel and Prieur, 1977) or at least other OACs such as CDOM and detrital particles covary with phytoplankton. For low concentrations, both band-ratio (R) and CI are inversely related to the total absorption coefficient (a(443), Eqs. 10 and 11), where the contribution of phytoplankton and CDOM/detrital particles to a(443) must covary in order to derive the former. There has been substantial evidence that the OACs often do not covary even for the open oceans [Loisel et al., 2002; Dierssen, 2010], which may explain why a globally optimized parameterization in OC4 may work well for one ocean basin or one season but its performance can be much worse for another [e.g., Gregg and Casey, 2004]. Thus, for global applications, one measure to assess algorithm robustness is to test its sensitivity to various scenarios where OACs do not covary.

For such a sensitivity analysis, the same approach of Lee et al. [2010] to assess IOP algorithm uncertainty was adapted here for both the OC4 and CIA. Synthetic data ($R_{rs}(\lambda)$ derived from various IOP combinations) were used to evaluate the impact of IOP variability on Chl retrieval accuracy.

Briefly, starting from Eq. (6), the geometric parameters ($G_0^w(\Omega), G_1^w(\Omega), G_0^p(\Omega)$, and $G_1^p(\Omega)$; sr^{-1}) were taken as (0.0604, 0.0406, 0.0402, 0.1310 sr^{-1}) [Lee et al 2011]. The absorption and backscattering coefficients were modeled as:

$$\begin{aligned} a(\lambda) &= a_w(\lambda) + a_{ph}(\lambda) + a_{dg}(\lambda) \\ b_b(\lambda) &= b_{bw}(\lambda) + b_{bp}(\lambda) \end{aligned}, \tag{13}$$

where $a_w(\lambda)$ and $b_{bw}(\lambda)$ are for water molecules and taken from Pope and Fry ([1997] and Morel [1974], respectively. $a_{ph}(\lambda)$, $a_{dg}(\lambda)$, and $b_{bp}(\lambda)$ are for phytoplankton pigments, detrital particles and CDOM, and particulate matter, respectively, and they are modeled as:

$$\begin{aligned} a_{ph}(\lambda) &= a_{ph}(440)\, a_{ph}^{+}(\lambda) \\ a_{dg}(\lambda) &= a_{dg}(440)\, e^{-S(\lambda-440)} \\ b_{\mathrm{bp}}(\lambda) &= b_{\mathrm{bp}}(440)\left(\frac{440}{\lambda}\right)^{\eta} \end{aligned}. \tag{14}$$

Here $a_{ph}^{+}(\lambda)$ is $a_{ph}(\lambda)$ normalized to $a_{ph}(440)$ and taken from the IOCCG [2006] database.

The dependence of $a_{dg}(\lambda)$ and $b_{bp}(\lambda)$ on Chl (or $a_{ph}(440)$) were defined as:

$$\begin{aligned} a_{dg}(440) &= p_1\, a_{ph}(440), \\ b_{bp}(440) &= 0.015 p_2\, Chl^{0.62}, \end{aligned} \tag{15}$$

where the exponent of 0.62 was taken from Gordon and Morel [1983], and 0.015 is the backscattering/total-scattering ratio [Sullivan and Twardowski, 2009].

For each Chl value (corresponding to an $a_{ph}(440)$), four parameters can be changed independently in modeling $R_{rs}(\lambda)$, and Chl can be retrieved from the modeled $R_{rs}(\lambda)$ with both OC4 and CIA (Eqs. 2-5) and compared with the input Chl to produce a relative error estimate. These four parameters include p_1, p_2, S, and η. Below we show the results of three scenarios.

Scenario 1. Both a_{dg} and b_{bp} vary independently from $a_{ph}(440)$

$a_{ph}(440)$ was set to 0.0028, 0.008, 0.024, and 0.05 m^{-1}, respectively, corresponding to Chl of 0.02, 0.05, 0.3, and 1.0 mg m^{-3}, respectively [Bricaud et al., 1995]. The minimum $a_{ph}(440)$ (0.0028 m^{-1}) is only half of the minimum $a_{ph}(440)$ in the IOCCG dataset, and approximates the $a_{ph}(440)$ values in the South Pacific Gyre [Morel et al., 2007b, Lee et al 2010]. For each $a_{ph}(440)$ (and its corresponding Chl), p_1 varied from 0.4 to 2.0 with a step of 0.1 (17 p_1 values); p_2 varied from 0.1 to 0.6 with a step of 0.1 (6 p_2 values); S varied from 0.013 to 0.019 with a step of 0.002 (4 S values); and η was set to 0.5 and 1.5. Thus, for each $a_{ph}(440)$ (Chl), there are 816 sets of a&b_b, 816 R_{rs} spectra, and 816 retrieved Chl values. The histogram of the relative errors of the 816 retrieved Chl values from each algorithm is shown in Fig. 6.

Except for the "high" concentration case (Chl = 1.0 mg m^{-3}), the performance of the two algorithms is similar. Most results showed relative errors to within ±50%. The CIA appears to yield less data points for errors > 60%, and appears to have a better performance (narrower histogram) for Chl = 0.3 mg m^{-3}.

Scenario 2. a_{dg} varies independently from $a_{ph}(440)$, but b_{bp} covaries with $a_{ph}(440)$

For each $a_{ph}(440)$, p_2 was set to 0.45, η = 1.0, S = 0.016, but p_1 was changed from 0.3 to 2.5 with a step 0.1 (23 p_1 values). Fig. 7a shows that the relative errors in the retrieved Chl from both algorithms change from negative to positive with increasing a_{dg}/a_{ph} ratios, an expected result where the increased CDOM/detrital particles were mistakenly regarded as Chl because they all strongly absorb the blue light. For extremely low concentrations (Chl < 0.1), errors from the CIA are slightly higher, but for higher concentrations the errors approach those from the OC4 algorithm. For the extreme case of Chl = 1.0 mg m^{-3}, errors from the CIA are lower than those from the OC4 algorithm, especially when $a_{dg}(440)/a_{ph}(440)$ is > 2.0 or < 1.0. In general, for Chl

≤ 0.25 mg m^{-3} and the moderate range of $a_{dg}(440)/a_{ph}(440)$ (1.0 – 2.0), the retrieval errors from the two algorithms are similar.

Scenario 3. b_{bp} varies independently from $a_{ph}(440)$, but a_{dg} covaries with $a_{ph}(440)$

For each $a_{ph}(440)$, p_1 was set to 1.0, η = 1.0, S = 0.016, but p_2 was changed from 0.1 to 0.6 with a step of 0.05 (21 p_2 values). Fig. 7b shows that for Chl < 0.3 mg m^{-3}, the CIA yielded much lower relative errors for all cases regardless of the error sign. The errors from the CIA change sign between 0.1 and 0.3 mg m^{-3}. At Chl = 0.4 mg m^{-3}, the CIA errors approach those from the OC4. At Chl = 1.0 mg m^{-3}, errors from the CIA are significantly higher than those from the OC4. These results suggest that for Chl < 0.4 mg m^{-3}, the performance of the CIA is often significantly better than the OC4v6 when b_{bp} varies independently from $a_{ph}(440)$ (or Chl).

The results above are based on simulated datasets, some of which may not be realistic in nature. Indeed, on large regional scales, the absorption OACs often covary [Morel, 2009], although their relative proportions in modulating the $R_{rs}(\lambda)$ may change from one ocean basin to another. For example, although the ratio of $a_{dg}(440)/a_{ph}(440)$ showed a weak seasonality in an oligotrophic ocean site and there was an observable temporal lag between the two absorption terms, they did show high correlations in the temporal patterns [Hu et al., 2006]. In contrast to absorption OACs, b_{bp} relative to Chl may vary substantially in both space and time [Loisel et al., 2002; Dierssen, 2010], where the CIA should perform significantly better than the OC4 algorithm in the algorithm tolerance to the independent b_{bp} changes for low concentration waters.

Overall, from these model-based simulations, we believe that the CIA should perform at least equivalently to the OC4 algorithm for Chl < 0.4 mg m^{-3}, if not significantly better. These results are also consistent to those shown in Fig. 3 when *in situ* data (assumed error free, but they certainly contained both measurement and data reduction errors) were used to evaluate algorithm performance, and consistent with those shown in Fig. 5.

6.3. Sensitivity to digitization-noise and atmospheric correction errors

The above simulations are based on the assumption that the inputs of the algorithms, namely the $R_{rs}(\lambda)$ data, are error free. In practice, $R_{rs}(\lambda)$ derived from satellite measurements may contain various errors from imperfect radiometric calibration, instrument noise and digitization round-off noise, imperfect atmospheric correction, residual errors from whitecap and sun glint corrections, and stray light contaminations (Eq. 1 and Fig. 1).

Assuming an error-free calibration and an error-free atmospheric correction scheme, Hu et al. [2001] used model simulations to evaluate the SeaWiFS data product uncertainties originating from instrument and digitization noise alone. They found that 1) errors in the retrieved $R_{rs}(\lambda)$ and band-ratio Chl were primarily from noise-induced perturbations in the atmospheric correction, which were propagated and enlarged from the near-IR bands to the visible bands, and 2) relative errors in the band-ratio Chl were more prominent in both low (< 0.1 mg m^{3}) and high (> 10 mg m^{3}) Chl ranges than in the intermediate Chl ranges.

The same simulations were applied here to compare relative errors in $\mathrm{Chl_{OC4}}$ and $\mathrm{Chl_{CI}}$ due to digitization/noise. Briefly, random noise at the level between $-0.5\delta(\lambda)$ and $0.5\delta(\lambda)$ was added to $\rho_t(\lambda)$ in Eq. (1), where $\delta(\lambda)$ is the spectral remote sensing reflectance corresponding to 1 digital count in the individual band:

$$\rho_t^{'}(\lambda) = \rho_t(\lambda) + \text{noise}. \qquad (16)$$

$\rho_t(\lambda)$ and $\rho_t^{'}(\lambda)$ were fed to the identical atmospheric correction and bio-optical inversion algorithms under various observation conditions (aerosol type and optical thickness, solar/viewing geometry), and the derived Chl from the noise-free $\rho_t(\lambda)$ and noise-added $\rho_t^{'}(\lambda)$ were compared and relative error assessed. Figs. 8 and 9 show examples of the simulation results. For 10,000 model runs of the given aerosol information (maritime aerosol with relative humidity of 90%) and solar/viewing geometry (scene center, solar zenith angle θ_o= 60°), the errors in the retrieved $R_{rs}(\lambda)$ due to digitization/noise alone are presented in Fig. 8. To first order, the errors are spectrally linear (Fig. 8a), and errors at 443 nm are roughly twice those at 555 nm (Fig. 8b). Because of the approximate linearity, most of these errors were cancelled in Eq. 3, resulting in much smaller errors in the CI (Fig. 8c). In contrast, these same $R_{rs}(\lambda)$ errors can only be cancelled to a lesser degree in the band ratio R (Eq. 2), especially when the ratio is significantly different from 2 (when the ratio is ~2, adding twice as much error in the numerator as in the denominator will make the ratio unchanged). For the oligotrophic oceans, $R_{rs}(555)$ is small (the blue/green ratio R may reach > 6.0 - 8.0), then large errors in the blue/green ratio could be resulted when $R_{rs}(\lambda)$ contains small, spectrally linear perturbations. Thus, the different sensitivity of R and CI to the digitization/noise induced errors leads to different accuracy in the retrieved Chl (Fig. 9). For the Chl range considered here, while the relative errors in Chl_{OC4} increased sharply with decreasing Chl, the errors in Chl_{CI} remained unchanged at a much lower level. Simulation results for other aerosol and solar/viewing geometry were different from those shown in Figs. 8 and 9, but the general pattern remained the same, i.e., relative errors in Chl_{OC4} were always higher than in Chl_{CI} for Chl < 0.4 mg mg^{-3}, with only the former depending on Chl.

Clearly, for Chl < 0.4 mg m^{-3}, Chl_{CI} is much less sensitive than Chl_{OC4} to digitization/noise induced errors for SeaWiFS. In practice, the atmospheric correction scheme implemented in SeaDAS has inherent errors to within ±0.002 in reflectance at 443 nm, which is the basis for the 5% fidelity in the retrieved reflectance at 443 nm for clear waters [Gordon and Wang, 1994a; Gordon, 1997]. The ±0.002 reflectance errors are equivalent to R_{rs}(443) errors of ~ ±0.002/π = ±0.0006 sr^{-1}, corresponding to R_{rs}(555) errors of about ±0.0003 sr^{-1}. These additional errors are comparable to those due to SeaWiFS digitization/noise (Figs. 8a & 8b) and are independent of instrument sensitivity (i.e., they apply to all ocean color sensors including SeaWiFS and MODIS/Aqua). While the digitization/noise induced errors, assumed randomly distributed, may be averaged out if sufficient number of points (image pixels) are available, the atmospheric correction errors may create a bias at various spatial and temporal scales because the conditions to result in these atmospheric correction errors may not be random (yet the spatial/temporal distributions of these conditions is unknown). This effect will be shown below with satellite data analysis.

7. Evaluation using SeaWiFS and MODIS/Aqua imagery

The CIA was applied to SeaWiFS Level-2 GAC data to derive Chl_{CI}, and compared with the default Chl_{OC4}. In the comparison, the following quality control flags were used to discard all suspicious data points: atmospheric correction failure (bit 1), land (bit 2), high sun glint (bit 4), total radiance greater than knee (bit 5), large satellite zenith (bit 6), stray light (bit 9), cloud/ice (bit 10), coccolithophores (bit 11), large solar zenith (bit 13), low water-leaving radiance (bit 15), chlorophyll algorithm failure (bit 16), questionable navigation (bit 17), near-IR exceeds maximum iteration (bit 20), chlorophyll warning (bit 22), and atmospheric correction warning (bit 23). These are the same flags as used to perform data quality control during SeaWiFS and

MODIS Level-3 data binning. Fig. 1 shows the images of Chl_{OC4}, Chl_{CI}, τ_865, and $R_{rs}(555)$ for the North Atlantic Ocean gyre from an arbitrarily selected date.

The image speckling effect is apparent in the Chl_{OC4} image (Fig. 1a), where discontinuity and patchiness can also be found. While the speckling effect (pixelization noise) is due primarily to digitization/noise induced errors, the patchiness is more likely due to atmospheric correction errors and other correction errors (such as whitecap correction). Indeed, similar discontinuity and patchiness are also found in the τ_865 and $R_{rs}(555)$ images (Figs. 1c and 1d). Such sharp changes and patchiness in both the atmosphere and ocean properties in an ocean gyre are unlikely to be realistic, but can only be due to algorithm errors. These errors occasionally led to $R_{rs}(555)$ values less than the theoretical limit for even the clearest ocean waters, 0.001 sr^{-1}. In contrast to the Chl_{OC4} image that contains speckle noise and patchiness, the Chl_{CI} image in Fig. 1b, derived from identical $R_{rs}(\lambda)$ data as used to derive Chl_{OC4}, shows much smoother and more spatially coherent distributions even near cloud edges. These results strongly suggest that Chl_{CI} is much more immune to both digitization/noise and atmospheric correction errors, consistent with those found from the simulations (Figs. 8 & 9). Note that some of the noises are due to straylight contamination near clouds, but most of these noises are effectively removed by the CIA, suggesting that these noises are also spectrally linear.

To quantify the image speckling noise from the satellite images, a 3x3 median filter was used to smooth the Chl images, with the result assumed as the "truth." The relative difference between the original data and the smoothed data was assumed to be primarily from digitization/noise induced errors. To avoid potential assessment bias due to insufficient sample size, all valid SeaWiFS Level-2 pixels for the 20^{o} x 20^{o} box in the North Atlantic gyre from the 599 images in 1998 were queried, and RMS error for each predefined Chl interval was calculated. Fig. 10a shows that the RMS errors in Chl_{OC4} increase sharply with decreasing Chl while these errors in Chl_{CI} remain stable at a much lower level. The overall patterns agree very well with those from the model simulations (Fig. 9), suggesting that most of these speckling errors originate from digitization/noise (through error propagation in the atmospheric correction). The discrepancy in the error magnitude between Fig. 9 and Fig. 10a originated from the different scenarios: Fig. 9 is for a single observing condition based on simulations while Fig. 10a accounts for all observing conditions for the entire year. Another reason may be due to stray light and imperfect sun glint and whitecap corrections, which were not accounted for in the simulations. Indeed, the SeaWiFS GAC data were collected by resampling the 1-km data every 4th row and column, and the potential small clouds between the resampled pixels may lead to stray light contamination to the "valid" pixels. These potential stray light problems for SeaWiFS GAC data cannot be assessed from the data alone because of the data gap (i.e., the resampled "1km" pixels in the GAC data are 3-km away from each other). Yet, Figs. 10a and 1 show that under realistic measurement conditions the relative RMS errors in Chl_{CI} is significantly smaller than in Chl_{OC4} for low concentrations. This finding holds true even when the SeaWiFS LAC data at 1-km resolution are used for the same comparison.

The statistics in Fig. 10a also suggest the improvement of the CI algorithm in reducing the number of "extreme" data points from the OC4 algorithm (e.g., Chl < 0.02 mg m^{-3}). These "extreme" points are not only due to digitization-induced errors, but also due to atmospheric correction errors and/or other algorithm artifacts (whitecap and sun glint corrections, stray light contamination). Indeed, the changes in the number of valid pixels for each Chl interval from Chl_{OC4} to Chl_{CI} suggest data redistribution, which will affect time-series analysis over low-concentration waters.

SeaWiFS data for the North Atlantic and South Pacific Gyres for an entire year were visualized to examine whether the above observations could be generalized. The results confirmed those shown in Fig. 1, and suggest that most digitization-noise related specking errors can be removed using the CIA for low concentrations, and many other algorithm artifacts (sun glint and whitecap corrections, atmospheric correction, and stray light contamination) can also be reduced with the CIA. The effect of such correction on time-series analysis is demonstrated below.

8. Comparison between Chl_{OC4} and Chl_{CI} time-series

Fig. 11 shows a one-year time-series at an oligotrophic site in the North Atlantic Gyre using SeaWiFS daily Level-2 GAC data. While the Chl_{OC4} data show high speckling (high standard deviations at each 3x3 point) and nearly no seasonality due to other errors, the Chl_{CI} data show much cleaner time series and also a clear seasonality. Note that the standard deviation at each point represents digitization/noise induced errors, but the deviation of the 3x3 mean data value from the seasonal pattern represents errors from other sources, which are effectively removed in the Chl_{CI} time series. This effect also remains for the monthly composite time series at the same location (Fig. 12). The seasonality of Chl_{CI} is clear in every year of the 13-year time series (note that there were some missing data after 2005 due to instrument operations), but less apparent in the corresponding Chl_{OC4} time series. The mean monthly variance (standard deviation over mean) reduced from 26.6% in Chl_{OC4} to 9.9% in Chl_{CI}. All these results suggest improvements of the CIA in constructing Chl time-series for oligotrophic waters.

The improvement of Chl_{CI} in deriving a better time series is primarily because of reduction of algorithm-induced errors as opposed to the reduction in speckling noise. As shown in Figs. 11 and 1 as well as in Hu et al. [2001], while the image speckling noise can be removed using pixel averaging (either 3x3 or temporal averaging), algorithm-induced errors cannot be removed this way and will ultimately propagate to higher-level data products in global or regional time-series analyses. The significantly reduced errors in the Chl_{CI} data product may result in more consistent spatial and temporal patterns than the current OC4 algorithm for the oligotrophic oceans.

9. Discussion

9.1. Algorithm accuracy: band ratio or band difference?

The comprehensive analyses above, from direct validation, theoretical background, sensitivity analysis through bio-optical and atmospheric correction simulations, to satellite data product comparison, all suggest that the CIA is more robust than the OC4 algorithm for low concentrations (Chl $\leq$ 0.25 mg m^{-3}). This range corresponds to about 77% of the global ocean area, suggesting potentially profound effects in global- and regional-scale studies. In particular, studies focusing on ocean gyre variability [McClain et al., 2004 et al., 2004; Polovina et al., 2004] and second-order ocean chlorophyll variability [Brown et al., 2008] may need to be revisited with the new algorithm.

The improved performance of the CIA is primarily due to two reasons. First, for most cases considered, it appears equivalent or even more tolerant (i.e. less sensitive) than the OC4 algorithm to in-water perturbations when the various OACs (especially particle backscattering) do not covary. Although the non-covariance of the OACs may represent a primary reason why a “global” algorithm may not work for a particular region [Claustre and Maritorena, 2003; Dierssen, 2010], it is not the objective of any empirical algorithm to solve this global “puzzle.” Likewise, the chlorophyll-specific absorption coefficient (i.e., absorption per Chl) may also vary substantially due to different pigment composition and phytoplankton size, but all "global" empirical algorithms would suffer the same from this variability. At the least, the CIA is equivalent or slightly better for most oligotrophic waters than the OC4 algorithm to the in-water perturbations. The improved performance over backscattering perturbations is of particular importance, as this may lead to an improved Chl retrieval in scattering-rich low-concentration waters due to bubbles or other marine organisms such as coccolithophores. Second and most importantly, the CIA can partially remove most algorithm artifacts induced by digitization-noise errors, atmospheric correction errors, residual errors due to imperfect sun glint and whitecap corrections, and some of the stray light contamination. Although the band-ratio OC4 algorithm can also remove some of these errors to a certain degree, the removal is much less effective for low-concentration waters.

Indeed, the concept to use alternative ways instead of band-ratio algorithms to derive Chl is not new. Campbell and Esaias [1983] proved why a curvature algorithm in the form of $S_j^2/(S_iS_k)$ could be used to derive chlorophyll concentrations. Here S_j represents the measured signal in one band (calibrated or not) and S_i and S_k represent the signals from the two neighboring bands. Barnard et al. [1999] showed the validity of a similar curvature approach to derive absorption coefficients. Lee and Carder [2000] further used simulations to compare band-ratio and band-curvature algorithm performance, and highlighted that band-ratio algorithms were more sensitive to a wider dynamic range.

Early pioneer efforts for algorithm development also proposed band-difference algorithms [Viollier et al., 1978; Viollier et al., 1980; Tassan, 1981], where the difference between two neighboring blue and green bands was related to surface Chl. The rationale for choosing a blue-green band difference was because of its tolerance to various errors in the spectral reflectance, including whitecaps [Tassan, 1981]. However, through model estimates, Gordon and Morel [1983] argued that because reflectance is in principle proportional to backscattering to the first order (i.e., $R_{rs} \propto b_b/a$, see Eq. 7), a band-difference algorithm will retain most variability of b_b relative to phytoplankton, thus subject to large errors if b_b varies independently from phytoplankton (e.g., sediment-rich coastal waters). In contrast, as long as the spectral variability of b_b is within a narrow range, a band-ratio algorithm will overcome such variability to first order, making the algorithm less sensitive to independent b_b changes. For this reason, except for a handful of studies in the 1980s, band difference algorithms have rarely been used in the published literature. One exception was perhaps the normalized difference pigment index (NDPI) algorithm proposed by Frouin [1997] for the POLarization and Directionality of the Earth's Reflectances (POLDER) instrument [Mukai et al., 2000], which combined the band-difference and band-ratio forms using the 443, 490, and 555-nm bands. The NDPI algorithm is essentially a band-ratio algorithm, although the 443-555 difference in the numerator has been shown to remove some noise. A similar combination of band-difference and band-ratio was proposed for the recently launched Geostationary Ocean Color Imager (GOCI), yet its performance over oligotrophic waters needs to be validated.

The fundamental principles and model simulation results in Sections 6.1 and 6.2 suggest that the arguments in Gordon and Morel [1983] on the weakness of band-difference algorithms should be revisited for oligotrophic oceans. Indeed, for Chl < 0.4 mg m^{-3}, the simulation results showed that a 3-band difference algorithm (i.e., the CIA) is more tolerant to independent b_b changes than the band-ratio algorithm. This may appear against intuition for the reasons outlined in Gordon and Morel [1983]. However, Eq. (6) shows that $R_{rs}(\lambda)$ is not proportional to particulate backscattering (b_{bp}), but influenced by both molecular and particle backscattering (b_{bw}) and b_{bp}. When Chl is low, the proportion of b_{bp} to total b_b is relatively small (e.g., $b_{bp}(440)$ ~35% of total $b_b(440)$ for Chl = 0.1 mg m^{-3}, and the other 65% is due to a constant water molecular scattering), resulting in the tolerance of the CIA to independent b_{bp} changes. In addition, the design of CI (Eq.3) places more relative weighting of b_{bw} than for b_{bp} for low concentrations. For high Chl waters (e.g., Chl = 1.0 mg m^{-3}, Fig. 7b), b_{bp} dominates b_b, and the CIA becomes more sensitive than the OC4 algorithm to independent b_{bp} changes, consistent with the arguments of Gordon and Morel [1983]. For the tolerance to other errors (sensor noise, atmospheric correction residual errors, sun glint and whitecap correction residual errors, stray light contamination, etc.), the CIA is better than the band-ratio algorithm, confirming Tassan's argument. The CIA, however, is not a simple blue-green difference, but takes a third band in the red to account for the various errors listed above.

The stability of empirical Chl algorithms to independent b_{bp} changes is particularly important to reduce Chl errors or inconsistencies either in one ocean basin or across multiple basins. Dierssen [2010] showed that for low Chl values (< 0.2-0.4 mg m^{-3}), $b_{bp}(532)$ may increase by several folds from the North Atlantic to the California coastal waters for the same Chl, and $b_{bp}(532)$ in the same ocean basin may also remain relatively stable when Chl varied substantially. Similarly, Loisel et al. [2002] showed seasonal shifts of $b_{bp}(490)$/Chl from SeaWiFS monthly data for both North Atlantic and North Pacific, with their relative ratios varying between ~0.6 and ~1.7 (x 10^{-2} (m^{-1} / mg m^{-3})), a change of about 3 folds. Fig. 7b suggests that for a 3-fold change between 0.175 and 0.525 on the x-axis, relative errors in Chl_{CI} are mostly within ±10% for Chl ≤ 0.3 mg m^{-3}, while the relative errors in Chl_{OC4} nearly doubled. Thus, the CIA can reduce backscattering induced errors in the Chl retrieval for oligotrophic waters.

Although the accuracy of the CIA appears to be higher than the OC4 algorithm for SeaWiFS (Fig. 4), it is indeed difficult to evaluate the absolute algorithm accuracy for low concentrations. This is primarily due to the lack of sufficient high-quality *in situ* data. The entire SeaBASS archive is restricted to Chl ≥ 0.02 mg m^{-3}, and only a limited number of stations had Chl between 0.02 and 0.05 mg m^{-3}. Laboratory measurement errors in determining Chl from seawater samples, using either fluorometric or HPLC methods, can be 50% [Trees, et al., 1985; Kumari, 2005]. The errors in these ground "truth" data further weaken the statistical robustness of the validation results when only several points are available. Future efforts may emphasize the oligotrophic ocean gyres to collect more *in situ* data in this range. Because most commercial instruments have a precision of about 0.01 mg m^{-3}, accurate laboratory measurement for this range is extremely difficult. While new sensors may be developed to increase the precision and accuracy, our current emphasis is on data consistency across various spatial and temporal scales, for which the CIA appears to yield better performance than the band-ratio algorithms.

Despite such improved performance in the CIA, all potential artifacts or uncertainties for empirical algorithms, as discussed and demonstrated in the refereed literature [IOCCG, 2000 & 2006; Dierssen, 2010], still exist (although to a less degree than band-ratio algorithms, as shown in the algorithm sensitivity to b_{bp} variability). Both CI and band-ratio provide a measure of the spectral change of R_{rs} (either difference or ratio). While most of such changes could be related to phytoplankton (i.e., Chl), they could also be modulated by changes in CDOM or other OACs. In addition, all these empirical algorithms assume, implicitly, a stable covariation of the chlorophyll-specific absorption coefficient with Chl. The ultimate way to improve Chl retrievals in the global oceans may still be to account for all these variability explicitly through semi-analytical inversions, but this is out of the scope of the present work. The semi-analytical algorithms, at least in their present forms, however, are not immune to the problems shown in Fig. 1d where R_{rs} data (input of the algorithms) contain substantial noise and errors. These errors must be corrected in order to improve the performance of semi-analytical algorithms. Likewise, algorithms for many other ocean color products (e.g. IOPs, particulate organic carbon or POC, particulate inorganic carbon or PIC) rely heavily on accurate $R_{rs}(\lambda)$, whose performance may also be improved once the errors in the satellite-derived $R_{rs}(\lambda)$ are reduced.

All above analysis were restricted to SeaWiFS GAC data. However, application of the same CIA algorithm to SeaWiFS LAC data showed similar improvements over image quality. Fig. 13 shows an example of the comparison of $\mathrm{Chl}_{\mathrm{OC4}}$ and $\mathrm{Chl}_{\mathrm{OCI}}$ using SeaWiFS Level-2 LAC data. Clearly, all instrument/algorithm artifacts shown in the GAC data (Fig. 1) also exist in the LAC data (to a lesser degree), but these artifacts can be effectively removed by the CIA algorithm.

9.2. Applications to other ocean color instruments

The improved performance in the CIA for low concentrations appears to be universal across sensors, although the regression coefficients may need to be adjusted to account for sensor specifics. Figs. 14-16 show several examples from other ocean color instruments, from MODIS/Aqua, MERIS, and CZCS, respectively, where improvement in image quality in terms of reduced noise/errors and image sharpness is apparent.

Similar to the SeaWiFS speckling error analysis shown in Fig. 10a, the same CIA was implemented to process all MODIS/Aqua Level-2 data for the 20° x 20° box in the South Pacific Gyre (745 images in 2002). Fig. 10b shows that, although the speckling errors are reduced for MODIS $\mathrm{Chl}_{\mathrm{OC3}}$ relative to SeaWiFS $\mathrm{Chl}_{\mathrm{OC4}}$ (MODIS/Aqua instrument signal-to-noise is about 2-3 times higher than SeaWiFS), the general pattern remains the same, i.e., increased specking errors with decreasing concentrations. MODIS $\mathrm{Chl}_{\mathrm{OCI}}$, in contrast, shows relatively stable and much lower specking errors. Nearly all data points in $\mathrm{Chl}_{\mathrm{OC3}} < 0.01$ mg m^{-3} have been raised in $\mathrm{Chl}_{\mathrm{OCI}}$, and this is likely to be real, as shown in the example in Fig. 13.

Fig. 13 shows that MODIS/Aqua $\mathrm{Chl}_{\mathrm{OC3}}$ data are not immune to noise and algorithm errors even after all suspicious data (associated with the various quality control flags) are discarded. In contrast, the CIA successfully "corrected" these suspicious data to reasonable levels, as gauged from nearby pixels and adjacent images. This result explains the histogram shift between Chl_{OC3} and Chl_{CI} for extremely low values in Fig. 10b. Furthermore, even when all the quality-control flags are turned off (i.e., all low-quality non-zero data are used), the CIA appears to perform well on all those flagged pixels (Figs. 13c&d), indicating that the $R_{rs}(\lambda)$ errors from those pixels are spectrally related so that the CIA could remove these errors, at least to the first order. This suggests that the CIA algorithm may also result in more spatial coverage, once appropriate flags are determined to relax the quality control criteria.

Fig. 15 shows an example of how the CIA (same coefficients used for SeaWiFS) improves MERIS image quality when compared with the default band-ratio algorithm. The reduction of pixelization and striping noise is apparent in the Chl_{OCI} image, with more coherent eddy features observed. More profound improvement has also been found for CZCS (Fig. 16). CZCS is an 8-bit instrument with much lower signal-to-noise ratio (about 3 times lower than SeaWiFS), and the band-ratio algorithm resulted in significant speckling noise and other errors (Fig. 16a), where no ocean feature can be observed. In contrast, most of these errors have been removed by the CIA, leading to clear eddy and circulation features in the North Atlantic oligotrophic ocean. Furthermore, the general gradient from west to east in Fig. 16a, a result of algorithm artifact, has been successfully removed in Fig. 16b.

Although the absolute accuracy in the retrieved Chl_{OCI} for other ocean color instruments has not been evaluated, we believe that once algorithm coefficients are tuned for the particular instruments or the satellite-derived $R_{rs}(\lambda)$ are tuned to the SeaWiFS wavelengths, a significant improvement in product accuracy, in addition to image quality can be achieved. Such an improvement may lead to more consistent observations between different instruments. For example, after a slight adjustment to convert the MODIS/Aqua $R_{rs}(547)$ to $R_{rs}(555)$ and application of the same CIA and coefficients (Eq. 4) to the global data for 2006, mean ratio between MODIS and SeaWiFS Chl over the global oligotrophic oceans shows much less seasonal variability and is closer to 1.0 from the CIA than from the OCx algorithms (Fig. 17). Such an improvement is even more profound when data distributions rather than a global mean ratio are examined. Fig. 18 shows the data distribution for all "deep" waters (> 200 m) from the band ratio (OCx) and CI algorithms using all SeaWiFS and MODIS/Aqua data collected during November 2006. Although there is a slight offset of 0.01-0.02 mg m^{-3} in the global mean and median values between the two algorithm results (a and b, respectively), the CIA (after blending with the OCx for Chl > 0.25 mg m^{-3}) resulted in nearly identical histograms between SeaWiFS and MODIS/Aqua measurements, a significant improvement in data cross-sensor data consistency as compared from those obtained from the OCx algorithms. Analyses for other months of 2006 showed similar improvements. Although we are still performing an extensive evaluation of the new algorithm for the global ocean using all SeaWiFS and MODIS/Aqua data, the improved consistency between SeaWiFS and MODIS/Aqua measurements from these preliminary results is indeed encouraging, and may eventually lead to a better multi-sensor Chl climate data record for long-term studies of ocean biological changes (Antoine et al., 2005; Gregg et al., 2005; Maritorena et al., 2010).

9.3. Other applications

Studies of the ocean's biogeochemistry call for the highest accuracy in data products. For many other applications, such a strict requirement may often be relaxed. For example, tracking of oil pollution requires timely knowledge on major ocean circulation features including eddies [Hu, 2011; Liu et al., 2011]. The various examples shown in Figs. 13-16 prove that the CIA can lead to significantly improved image quality for feature recognition when individual images are used. This is due to its ability to reduce noise and errors as well as to "recover" most of the flagged (i.e., suspicious) pixels. Some of the eddy features are completely absent in the Chl_{OCx} images due to noise and algorithm errors (i.e., regardless of the color stretch), but are vividly revealed in the Chl_{OCI} images. This ability will greatly facilitate studies of eddy dynamics (e.g., Lehahn et al., 2007; Rossby et al., submitted) in the oligotrophic oceans.

10. Conclusion

A novel 3-band reflectance difference algorithm, namely a color index algorithm (CIA), to estimate surface chlorophyll-a concentrations from satellite ocean color measurements has been shown superior to the existing band-ratio algorithms in reducing uncertainties for Chl ≤ 0.25 mg m^{-3}, corresponding to about 77% of the global ocean. This was somehow a surprise, given the known artifacts of 2-band difference algorithms proposed three decades ago. We attribute the success of the CIA to the new design of adding a third band in the red to the blue-green bands.

This addition enables the CIA to relax the requirements of spectrally flat errors for the 2-band difference algorithms to spectrally linear errors for the CIA, and also increases the stability of algorithm performance over backscattering variability of the ocean. The improved performance of the CIA over the existing band-ratio algorithms has been demonstrated in all measures, from global validations using *in situ* data, atmospheric correction and bio-optical simulations, to satellite image analysis. The CIA also appears to improve data consistency between different instruments for oligotrophic oceans. We expect to implement the CIA for multi-sensor global processing for oligotrophic oceans to further test its robustness, which might lead to different and potentially improved spatial/temporal patterns of Chl in response to long-term climate changes and short-term climate variability.

Acknowledgement

This work is impossible without the collective effort from the entire ocean color community, from sensor calibration, field campaign, algorithm development, product validation, to data sharing. We are particularly thankful to the researchers who collected and contributed *in situ* bio-optical data to the SeaBASS archive, as well as to the NASA/GSFC OBPG team (Sean Bailey and Jeremy Werdell) who quality-controlled, maintained, and distributed the dataset for community use. We also thank the NASA/GSFC for sharing the global ocean color data at all data levels. Financial support has been provided by the NASA Ocean Biology and Biogeochemistry (OBB) program (Hu, Lee, Franz) and Energy and Water Cycle program (Lee, Hu), and the Naval Research Lab (Lee).

References

Ahmad, Z., B. A. Franz, C. R. Charles, E. J. Kwiatkowska, J. Werdell, E. P. Shettle, and B. N. Holben (2010) New aerosol models for the retrieval of aerosol optical thickness and normalized water-leaving radiances from the SeaWiFS and MODIS sensors over coastal regions and open oceans. Appl. Opt. 49:5545-5560.

Antoine, D., A. Morel, H. R. Gordon, V. F. Banzon, and R. H. Evans (2005). Bridging ocean color observations of the 1980s and 2000s in search of long-term trends. *J. Geophys. Res.*, 10.1029/2004JC002620.

Arvesen, J. C., J. P. Millard, and E. C. Weaver (1973). Remote sensing of chlorophyll and temperature in marine and fresh waters. *Astronaut. Acta.*, 18:229-239.

Bailey, S. W., B. A. Franz, and P. J. Werdell (2010). Estimation of near-infrared water-leaving reflectance for satellite ocean color data processing. *Optics Express, 18,* 7521-7527

Barnard, A. H., J. R. Zaneveld, and W. S. Pegau (1999). In situ determination of the remotely sensed reflectance and the absorption coefficient: closure and inversion. *Appl. Opt.* 38:5108–5117.

Behrenfeld, M., R. O'Malley, D. A. Siegel, C. R. McClain, J. Sarmiento, G. Feldman, P. Falkowski, E. Boss, and A. Milligan (2006). Climate-driven trends in contemporary ocean productivity. *Nature*, 444:752-755.

Bricaud, A., M. Babin, A. Morel, and H. Claustre (1995). Variability in the chlorophyll-specific absorption coefficients of natural phytoplankton: Analysis and parameterization, J. Geophys. Res., 100(C7), 13321-13332.

Brown, C., Y. Huot, P.J. Werdell, B. Gentili, and H. Claustre (2008). The origin and global distribution of second order variability in satellite ocean color. Remote Sens. Environ 112:4186-4203.

Campbell, J. W., and W. E. Esaias (1983). Basis for spectral curvature algorithms in remote sensing of chlorophyll. *Appl. Opt.* 22:1084–1093.

Campbell, J. W. (1995). The lognormal distribution as a model for bio-optical variability in the sea, J. Geophys. Rex, Vol. 100, No. C7, pp. 13237-13254.

Carder, K. L., F. R. Chen, Z. P. Lee, S. K. Hawes, and D. Kamykowski (1999) Semianalytic moderate-resolution imaging spectrometer algorithms for chlorophyll a and absorption with bio-optical domains based on nitrate-depletion temperatures. *J. Geophys. Res.*, 104:5403–5421.

Clark, D. K., E. T. Baker, and A. E. Strong (1980). Upwelled spectral radiance distribution in relation to particulate matter in sea water. Boundary Layer Meteorology, 18:287-298.

Clarke, G. K., G. C. Ewing, and C. J. Lorenzen (1970). Spectra of backscattered light from the sea obtained from aircraft as a measure of chlorophyll concentration. *Science*, 167:1119-1121.

Claustre, H., and S. Maritorena (2003). The many shades of ocean blue. *Science*, 302:1514-1515.

Dierssen, H. M., R. C. Smith, and M. Vernet (2002). Glacial meltwater dynamics in coastal waters west of the Antarctic peninsula. Proc Natl Acad Sci USA 99: 1790–1795.

Dierssen, H. M. (2010). Perspectives on empirical approaches for ocean color remote sensing of chlorophyll in a changing climate. Proc. Nat Acad Sci. 107:17073-17078.

Franz, B. A., S. W. Bailey, P. J. Werdell, and C. R. McClain (2007). Sensor-independent approach to the vicarious calibration of satellite ocean color radiometry. *Appol. Opt.* 46:5068-5082.

Frouin, R., M. Schwindling, and P.-Y. Deschamps (1996). Spectral reflectance of sea foam in the visible and near-infrared: In situ measurements and remote sensing implications. *J. Geophys. Res.,* 101:14,361-14,371.

Frouin, R. (1997). NDPI for satellite ocean color applications, in: Proceedings of the Fourth IPSWT, Boussens, France, 1997.

Gordon, H. R., and D. K. Clark (1980). Remote sensing optical properties of a stratified ocean: an improved interpretation. Appl. Opt. 19:3428-3430.

Gordon, H. R. and D. K. Clark (1981). Clear water radiances for atmospheric correction of coastal zone color scanner imagery. *Appl. Opt.* 20:4175-4180.

Gordon, H. R, and A. Y. Morel (1983). Remote assessment of ocean color for interpretation of satellite visible imagery. A Review. Springer-Verlag, New Work, Berlin, Heidelberg, Tokyo. 114 pp.

Gordon, H. R., and Wang, M. (1994a), Retrieval of water-leaving radiance and aerosol optical thickness over the oceans with SeaWiFS: a preliminary algorithm. *Appl. Opt.* 33:443-452.

Gordon, H. R., and Wang, M. (1994b), Influence of oceanic whitecaps on atmospheric correction of SeaWiFS. *Appl. Opt.* 33:7754-7763.

Gordon, H.R. (1997). Atmospheric correction of ocean color imagery in the Earth Observing System era. *J. Geophys. Res., 102,* 17081-17106.

Gower, J., S. King, and G.Borstad, et al. (2005).Detection of Intense Plankton Blooms Using the 709nm Band of the Meris Imaging Spectrometer. *Int. J. Remote Sens.* 26:2005-2012.

Gregg, W.W., N. W. Casey (2004). Global and regional evaluation of the SeaWiFS chlorophyll dataset. *Remote Sens. Environ.*, 93:463-479.

Gregg, W. W., N. W. Casey, and C. R., McClain (2005). Recent trends in global ocean chlorophyll. *Geophys. Res. Lett.*, 32, L03606, doi:10.1029/2004GL021808.

Hovis, W. A., and K. C. Leung (1977). Remote sensing of ocean color. *Optical Engineering*, 16:153-166.

Hu, C., Carder, K. L, and Muller-Karger, F. E. (2001), How precise are SeaWiFS ocean color estimates? Implications of digitization-noise errors, *Remote Sens. Environ.* 76:239-249.

Hu, C., Muller-Karger, F. E., Biggs, D. C., Carder, K. L., Nababan, B., Nadeau, D., and Vanderbloemen, J. (2003), Comparison of ship and satellite bio-optical measurements on the continental margin of the NE Gulf of Mexico, *Int. J. Remote Sens.* 24:2597-2612.

Hu, C., Z. Lee, F. E. Muller-Karger, K. L. Carder, and J. J. Walsh (2006). Ocean color reveals phase shift between marine plants and yellow substance. *IEEE Geoscience and Remote Sens. Lett.* 3:262-266.

Hu, C. (2009). A novel ocean color index to detect floating algae in the global oceans. *Remote Sens. Environ.* 113 :2118 :2129.

Hu, C. (2011). An empirical approach to derive MODIS ocean color patterns under severe sun glint. *Geophys. Res. Lett.*, 38, L01603, doi:10.1029/2010GL045422.

IOCCG (2000). Remote sensing of ocean color in coastal, and other optically-complex, waters. Reports of the International Ocean-Colour Coordinating Group, No. 3, Sathyendranath, S. (eds), Dartmouth, Canada. IOCCG.

IOCCG (2006). Remote Sensing of Inherent Optical Properties: Fundamentals, Tests of Algorithms, and Applications. Reports of the International Ocean-Colour Coordinating Group, No. 5. Z.-P. Lee. Dartmouth, Canada, IOCCG.

Kahru, M., and B.G. Mitchell (1999). Empirical chlorophyll algorithm and preliminary SeaWiFS validation for the California Current. *Int. J. Remote Sens.*, 20, N17, 3423-3429.

Kumari, B. (2005) Comparison of high performance liquid chromatography and fluorometric ocean colour pigments. J. Ind. Soc. Remote Sens., 33:541–546.

Lee, Z., and K. L. Carder (2000). Band-ratio or spectral-curvature algorithms for satellite remote sensing? *Appl. Opt.* 39:4377-4380.

Lee, Z., R. Arnone, C. Hu, P. J. Werdell, and B. Lubac. (2010). Uncertainties of optical parameters and their propagations in an analytical ocean color inversion algorithm. *Appl. Opt.* 49:369-381.

Lee, Z.-P., K. Du, K. Voss, G. Zibordi, B. Lubac, R. Arnone, A. Weidemann (2011). An IOP-centered approach to correct the angular effects in water-leaving radiance. *Appl. Opt.*, in press.

Lehahn, Y., F. d'Ovidio, M. Levy, and E. Heifetz (2007), Stirring of the northeast Atlantic spring bloom: A Lagrangian analysis based on multisatellite data. J. Geophys. Res., 112, C08005, doi:10.1029/2006JC003927.

Letelier, R. M., and M. R. Abott (1996). An analysis of chlorophyll fluorescence algorithms for the Moderate Resolution Imaging Spectrometer (MODIS). *Remote Sens. Environ.* 58:215–223.

Loisel, H., J.-M. Nicolas, P.-Y. Deschamps, and R. Frouin (2002). Seasonal and inter-annual variability of particulate organic matter in the global ocean. Geophys. Res. Lett., vol. 29, no. 24, p. 2196, 2002, DOI: 10.1029/2002GL015948.

Marrari, M., C. Hu, and K. Daly (2006). Validation of SeaWiFS chlorophyll-a concentrations in the Southern Ocean: A revisit. *Remote Sens. Environ.* 105:367-375.

Maritorena, S., D.A. Siegel and A. Peterson (2002). Otimization of a semi-analytical ocean color model for global scale applications. Appl. Opt., 41:2705-2714.

Maritorena S., O. Hembise Fanton d'Andon, A. Mangin, and D.A. Siegel (2010). Merged satellite ocean color data products using a bio-optical model: Characteristics, benefits and issues. *Remote Sens. Environ.,* 114, 8: 1791-1804.

McClain, C. R., G. C. Feldman, and S. B. Hooker (2004). An overview of the SeaWiFS project and strategies for producing a climate research quality global ocean bio-optical time series. Deep-Sea Research II, 51, 5-42.

McClain, C. R., S. R. Signorini, and J. R. Christian (2004). Subtropical gyre variability observed by ocean-color satellites. *Deep Sea Res., Part II,* 51:281-301.

McClain, C. R. (2009). A decade of satellite ocean color observations. Annu Rev Mar Sci 1:19–42.

McKee, D., A. Cunningham, and A. Dudek (2007). Optical water type discrimination and tuning remote sensing band-ratio algorithms: Application to retrieval of chlorophyll and $K_d(490)$ in the Irish and Celtic Seas. *Estuarine, Coastal, and Shelf Science*, 73:827-834.

Mitchell, B. G., and M. Kahru (2009). Bio-optical algorithms for ADEOS-2 GLI. *Journal of The Remote Sensing Society of Japan*. 29:80-85.

Morel, A. (1974). Optical properties of pure water and pure sea water. Optical Aspects of Oceanography. N. G. Jerlov, and Nielsen, E. S. New York, Academic: 1-24.

Morel, A. Y., and L. Prieur (1977). Analysis of variations in ocean color. *Limnol. Oceanogr.*, 22:709-722.

Morel, A. Y. (1980). In-water and remote measurement of ocean color. Boundary Layer Meteorology, 18:177-201.

Morel, A. and B. Gentili (1993). Diffuse reflectance of oceanic waters (2): Bi-directional aspects. Applied Optics 32: 6864-6879.

Morel, A., and S. Maritorena (2001). Bio-optical properties of oceanic waters: A reappraisal. *J. Geophys. Res.*, 106:7163-7180.

Morel, A., Y. Huot, B. Gentili, P. J. Werdell, S. B. Hooker, and B.A. Franz (2007a). Examining the consistency of products derived from various ocean color sensors in open ocean (Case 1) waters in the perspective of a multi-sensor approach. *Remote Sensing of Environment*, 111:69-88.

Morel, A., B. Gentili,H. Claustre, M. Babin, A. Bricaud, J. Ras, and F. Tieche (2007b). Optical properties of the "clearest" natural waters. Limnol. Oceanogr. 52(1): 217-229.

Mukai, S., I. Sano, and Y. Okada (2000). Inverse problems in the atmosphere–ocean system: estimation of aerosol characteristics and phytoplankton distribution. Applied Mathematics and Computation. 116:93-101, doi:10.1016/S0096-3003(99)00197-6.

Odriozola, A. L., R. Varela, C. Hu, Y. Astor, L. Lorenzoni, and F. E. Muller-Karger (2007). On the absorption of light in the Orinoco River plume. *Cont. Shelf Res.* 27:1447-1464.

O'Reilly, J. E, et al. (2000) SeaWiFS Postlaunch Calibration and Validation Analyses, Part 3. NASA Tech. Memo. 2000-206892, eds Hooker SB, Firestone ER, (NASA Goddard Space Flight Center), Vol 11, 49 pp.

Polovina, J. J., E. A. Howell, and M. Abecassis (2008). Ocean's least productive waters are expanding. *Geophys. Re. Lett.*, 35, L03618, doi:10.1029/2007GL031745.

Pope, R., and E. Fry (1997). Absorption spectrum (380 - 700 nm) of pure waters: II. Integrating cavity measurements. *Appl. Opt.*, 36:8710-8723.

Rossby, T., C. Flagg, P. Ortner, and C. Hu (submitted). A tale of two eddies: Diagnosing coherent eddies through acoustic remote sensing. *J. Geophys. Res.*

Sathyendranath, S., L. Prieur, and A. More (1989). A three component model of ocean colour and its application to remote sensing of phytoplankton pigments in coastal waters. Int. J. Remote Sens., 10:1373–1394.

Sullivan, J. M. and M. S. Twardowski (2009). Angular shape of the oceanic particulate volume scattering function in the backward direction. Applied Optics 48(35): 6811-6819.

Tassan, S. (1981). A global sensitivity analysis for the retrieval of chlorophyll concentrations from remote sensed radiances – the influence of wind. In: Oceanography from Space, edited by J. R. F. Gower. Plenum Press, New York, p.371-376.

Trees, C. C., M. C. Kennicutt, and M. J. Brooks (1985). Errors associated with the standard fluorometric determination of chlorophylls and phaeopigments. Mar. Chem 17:1–12.

Viollier, M., P. Y. Deschamps, and P. Lecomte (1978). Airborne remote sensing of chlorophyll content under cloudy sky as applied to the tropical waters in the Gulf of Guinea. *Remote Sens. Environ.* 7:235-248.

Viollier, M., D. Tanre, and P. Y. Deschamps (1980). An algorithm for remote sensing of water color from space. *Boundary Layer Meteorology*, 18:247-267.

Wang, M., and S. W. Bailey (2001). Correction of sun glint contamination on the SeaWiFS ocean and atmosphere products. *Appl. Opt.* 40:4790-4798.

Werdell, P. J., and S. W. Bailey (2005). An improved in-situ bio-optical data set for ocean color algorithm development and satellite data product validation. *Remote Sens. Environ.*, 98:122-140.

Yoder, J. A., and M. A. Kennelly (2006). What have we learned about ocean variability from satellite ocean color imagers? *Oceanography*, 19: 152 – 171.

Tables

Table 1. Chl algorithm performance for CI < -0.0005 sr^{-1} using the NOMAD dataset. OC_{low} represents a local polynomial fit between the log-transformed band-ratio and Chl for low concentrations only (CI < -0.0005, Fig. 3a red line), which shows improved performance than the globally tuned OC4v6. The regression equation is $Chl_{OC\_low} = 10.^{-0.39064 - 1.54789\chi + 3.2125*\chi*\chi - 3.1073*\chi*\chi*\chi}$. URMS is "unbiased" RMS (see text for details).

Algorithm	**RMS**	**URMS**	**Mean Ratio**	**Median Ratio**	**R^2** (linear)	**R^2** (log)	**N**
OC4v6	34.9%	28.2%	1.11	1.08	0.73	0.85	50
CI	**16.5%**	**16.2%**	**1.01**	**1.01**	**0.78**	**0.95**	**50**
OC_{low}	22.7%	22.3%	1.03	1.05	0.73	0.85	50

Table 2. Chl algorithm performance for Chl ≤ 0.25 mg m^{-3}, as gauged by *in situ* Chl (Fig. 4). SeaWiFS-derived $R_{rs}(\lambda)$ were used as the input of all algorithms. OC_{low} represents a local band-ratio algorithm for low concentrations only (CI < -0.0005 sr^{-1}, Fig. 3a red line). MRE is the mean relative error after converting negative errors to positive. URMS is "unbiased" RMS (see text for details).

Alg.	**RMS**	**URMS**	**Mean Ratio**	**Median Ratio**	**MRE**	**R^2** (linear)	**R^2** (log)	**N**
OC4v6	535.8%	54.2%	1.79	1.19	41.5%	0.01	0.33	357
CI	**91.8%**	**47.2%**	**1.40**	**1.16**	**36.8%**	**0.31**	**0.39**	**357**
OC_{low}	92.9%	45.6%	1.33	1.08	34.7%	0.20	0.36	357

Figure captions

Fig. 1. SeaWiFS Level-2 GAC data products at 4-km resolution on 20 February 1998 over the Sargasso Sea (about 1800 x 2640 km centered at 25.5^{o}N 54.8^{o}W). (a) Chl derived from the default OC4v6 algorithm (Chl_{OC4}); (b) Chl derived from a new color-index (CI) based algorithm (Chl_{CI}, see text for details); (c) Aerosol optical thickness at 865 nm (τ_865, dimensionless); (d) Remote sensing reflectance at 555 nm ($R_{rs}(555)$, x10^3 sr^{-1}). All suspicious data, as defined by the various Level-2 flags, have already been removed (black color).

Fig. 2. Illustration of the CI algorithm concept. When Chl increases from 0.02 to 0.33 mg m^{-3}, $R_{rs}(443)$ decreases while $R_{rs}(555)$ and $R_{rs}(670)$ remain relatively stable. Thus, the distance from $R_{rs}(555)$ to the linear baseline between $R_{rs}(443)$ and $R_{rs}(670)$ (dotted line in the figure), defined as the color index (CI), is highly corrected with Chl. This is the same principle as using the $R_{rs}(443)$/ $R_{rs}(555)$ ratio to relate to Chl. These *in situ* data are from the NOMAD dataset.

Fig. 3. Relationship between *in situ* chlorophyll-a concentration (Chl) and (a) reflectance ratio *R* and (b) color index (CI). The highlighted points emphasize those corresponding to CI ≤ -0.0005, where the corresponding data collection locations are shown in the inset map. Note that the minimum Chl in this dataset is about 0.02 mg m^{-3}. In (a), the RMS error is estimated between measured and OC4v6 predicted Chl. If a best fit from all data points for CI < -0.0005 sr^{-1} is used, RMS error is reduced to 22.95%. Statistics are presented in Table 1.

Fig. 4. Comparison between *in situ* Chl and satellite-based Chl for SeaWiFS. The satellite Chl was derived from both the OC4v6 algorithm (empty circles) and OCI algorithm (dots). Note that for Chl > 0.4 mg m^{-3} the results from the two algorithms were forced to be identical (Eq. 5). The locations of the *in situ* measurements for Chl ≤ 0.25 mg m^{-3} are shown in the corresponding map. The comparison statistics for low concentration (Chl ≤ 0.25) are listed in Table 2.

Fig. 5. Relationship between the two backscattering terms in Eq. (9) with Chl. To show their relative magnitudes, the absolute values (x 1000) are shown here. Note that for Chl ≤ 0.4 mg m^{-3}, the water term dominates the numerator of Eq. (9).

Fig. 6. Chl algorithm sensitivity to independent changes of detrital particles and CDOM relative to phytoplankton, based on 816 model simulations for each Chl value (Eq. 6, 13-15).

Fig. 7. Chl algorithm sensitivity to independent changes of absorption of detrital particles and CDOM (a_{dg}) relative to Chl (a), and to independent changes of particular backscattering (b_{bp}) relative to Chl (b), based on model simulations for each Chl value (Eq. 6, 13-15). Note that in (b), the added simulation was for Chl = 0.4 (star symbols), when the errors in the CI retrievals are shown to approach those of the OC4 retrievals.

Fig. 8. Errors in $R_{rs}(\lambda)$ and CI induced by SeaWiFS digitization-noise after applying the Gordon and Wang (1994a) atmospheric correction. Most of the errors are due to the impact of the small noise on the atmospheric correction bands in the near infrared, which extrapolate the atmospheric properties to the visible (Hu et al., 2001). These errors are approximately linear to changing wavelengths (a and b), and can thus be corrected to first order by the CI algorithm (Eq. 3, Fig. 2), resulting in smaller errors in CI (and Chl_{CI}, see Fig. 9). The model parameters are listed in (c). Results from other modeling scenarios are different, but the principles in reducing the noise-reduced errors using the CI are the same.

Fig. 9. Error distribution in the retrieved Chl due to digitization-noise induced $R_{rs}(\lambda)$ errors for a clear maritime atmosphere (Fig. 8). *In situ* R_{rs} data for the input Chl concentrations (from 0.02 to 0.4 mg m^{-3}) were combined with the $R_{rs}(\lambda)$ errors to estimate Chl, where the "true" Chl was determined from the input R_{rs} data free of errors. The differences were used to determine the relative retrieval errors. Note that the CI-based retrieval errors are independent of Chl concentrations.

Fig. 10. (a) Statistics of speckling error in SeaWiFS GAC images in 1998 (n=599) for a 20 x 20^{o} region in the Sargasso Sea. The speckling error is defined as the relative difference between the original Level-2 Chl and a 3x3 median-filter smoothed Level-2 Chl, with the assumption that most noise-induced speckling errors are removed in the latter. Note that while the RMS errors in Chl_{OC4} increase sharply with decreasing concentrations, RMS errors in Chl_{CI} remain stable at a much lower level in the entire concentration range here. The overall patterns agree well with those from the model simulations (Fig. 9), suggesting that most of these speckling errors originate from digitization/noise (through atmospheric correction). The total number of valid pixels from each algorithm indicates that all $Chl_{OC4} \leq 0.02$ mg m^{-3} appear unrealistic due to primarily atmospheric correction artifacts. (b) Same as in (a), but data were extracted from MODIS/Aqua Level-2 images in 2002 (n=745) for a 20 x 20^{o} subregion in the Southern Pacific.

Fig. 11. Chl (mg m^{-3}) time series derived from SeaWiFS GAC $R_{rs}(\lambda)$ data using the OC4v6 algorithm (top) and the CI algorithm (bottom). Data were extracted from 3x3 pixels centered at 24.5°N 55°W from the daily measurements. For any given image (date), only when more than half of the pixels (in this case, ≥5 pixels) contained valid data (i.e., not associated with any suspicious flags) were statistics estimated.

Fig. 12. Chl (mg m^{-3}) time series derived from SeaWiFS GAC $R_{rs}(\lambda)$ data using the OC4v6 algorithm (top) and the CI algorithm (bottom). Data were first extracted from 3x3 pixels centered at 24.5°N 55°W from the daily measurements. For any given image (date), only when more than half of the pixels (in this case, ≥5 pixels) contained valid data (i.e., not associated with any suspicious flags) were statistics estimated. The daily data were then averaged for the calendar month to construct the monthly time series. Note that SeaWiFS was not continuously operational after 2005 due to instrument operations.

Fig. 13. Comparison between SeaWiFS Level-2 Chl_{OC4} (a) and Chl_{OCI} (b) over the western North Atlantic Ocean. SeaWiFS data were collected on 1 June 2004 (17:15 GMT) and processed with SeaDAS6.1. The Level-2 quality-control flags were turned off to show the circulation features. Note that some eddy features are clearly revealed in the Chl_{OCI} image but absent in the Chl_{OC4} image due to noise and residual errors in atmospheric correction and other corrections.

Fig. 14. MODIS/Aqua Level 2 Chl_{OC3} and Chl_{OCI} derived from a subregion in the South Pacific Gyre (about 2200 x 440 km centered at 25.2°S 110.8°W) on 4 March 2003, 21:10 GMT. (a) and (c) show the default Chl_{OC3} when the quality control flags are on and off, respectively. (b) and (d) are the corresponding Chl_{OCI} images.

Fig. 15. Comparison between MERIS full-resolution (FR) Chl_{OC3} (a) and Chl_{OCI} (b) over the western North Atlantic Ocean. MERIS data were collected on 7 May 2011 (15:21 GMT) and processed with SeaDAS6.1. Note that most speckling and vertical striping noise in the Chl_{OC3} image has been removed in the Chl_{OCI} image, where several eddy and circulation features can be better observed. Further, although the same algorithm coefficients for SeaWiFS were used, Chl_{OCI} values in offshore water appear to be closer than Chl_{OC3} to those from SeaWiFS for the same region during similar periods (Fig. 13).

Fig. 16. Comparison between CZCS Level-2 Chl_{OC2} (a) and Chl_{OCI} (b) over the western North Atlantic Ocean (about 30^o – 36^{o}N, 70^o – 60^{o}W). CZCS data were collected on 31 July 1983 (16:02 GMT) and processed with SeaDAS6.1. Note that all eddy and circulation features in the Chl_{OCI} image are completely absent in the Chl_{OC2} image.

Fig. 17. Mean Chl ratio over global oligotrophic oceans between MODIS/Aqua and SeaWiFS estimates using the OCx (blue) and CI (black) algorithms. Here “oligotrophic” is defined as all 9-km pixels with SeaWiFS mission mean Chl $\leq$ 0.1 mg m^{-3}.

Fig. 18. Chl distribution in the global deep oceans (> 200 m) during November 2006, as derived from SeaWiFS (black) and MODIS/Aqua (red) measurements. Results in (a) are from the OCx band-ratio algorithms, and in (b) are from the CI algorithm (blended with the OCx algorithms for Chl > 0.25 mg m^{-3}). Note the offset of 0.01 – 0.02 mg m^{-3} in the global mean and median values between (a) and (b). Results from other months of 2006 show similar improvements in histogram consistency.

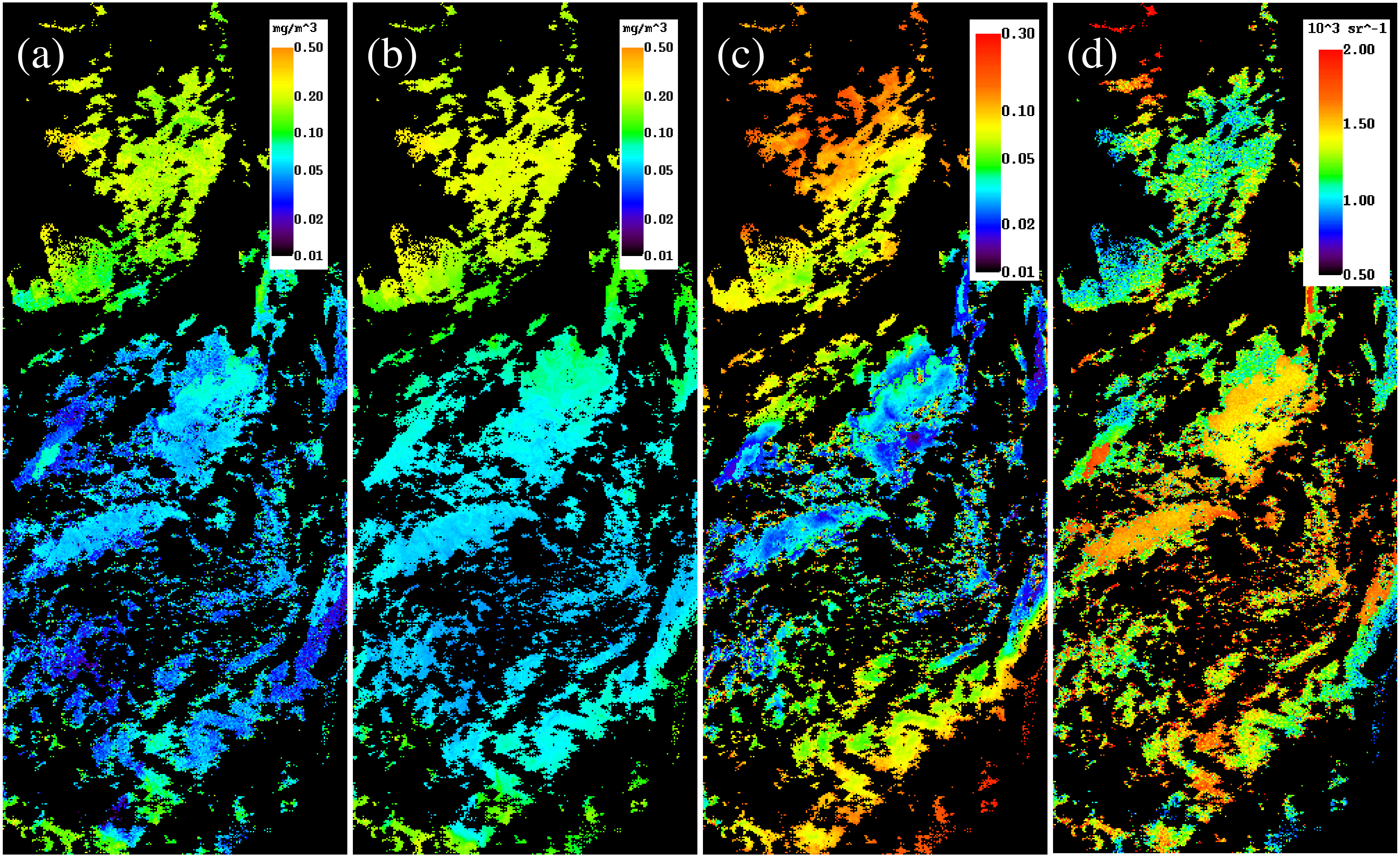

Fig. 1. SeaWiFS Level-2 GAC data products at 4-km resolution on 20 February 1998 over the Sargasso Sea (about 1800 x 2640 km centered at 25.5°N 54.8°W). (a) Chl derived from the default OC4v6 algorithm (Chl_{OC4}); (b) Chl derived from a new color-index (CI) based algorithm (Chl_{CI}, see text for details); (c) Aerosol optical thickness at 865 nm (τ_865, dimensionless); (d) Remote sensing reflectance at 555 nm ($R_{rs}(555)$, x10^3 sr^{-1}). All suspicious data, as defined by the various Level-2 flags, have already been removed (black color).

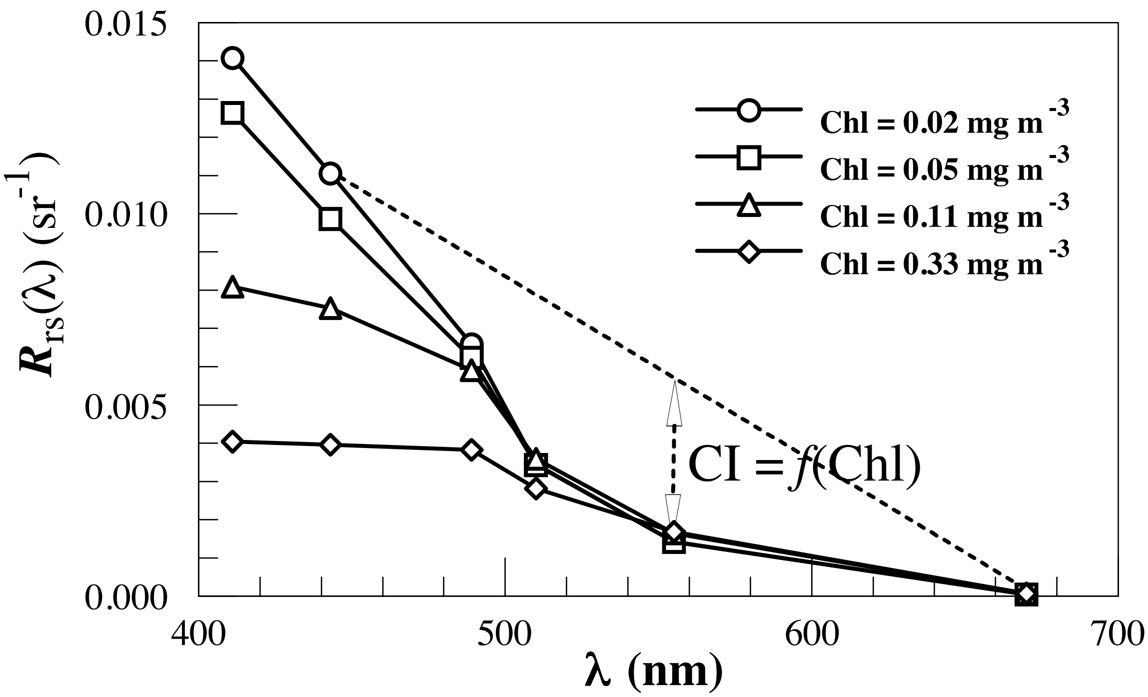

Fig. 2. Illustration of the CI algorithm concept. When Chl increases from 0.02 to 0.33 mg m^{-3}, $R_{rs}(443)$ decreases while $R_{rs}(555)$ and $R_{rs}(670)$ remain relatively stable. Thus, the distance from $R_{rs}(555)$ to the linear baseline between $R_{rs}(443)$ and $R_{rs}(670)$ (dotted line in the figure), defined as the color index (CI), is highly corrected with Chl. This is the same principle as using the $R_{rs}(443)$/ $R_{rs}(555)$ ratio to relate to Chl. These *in situ* data are from the NOMAD dataset.

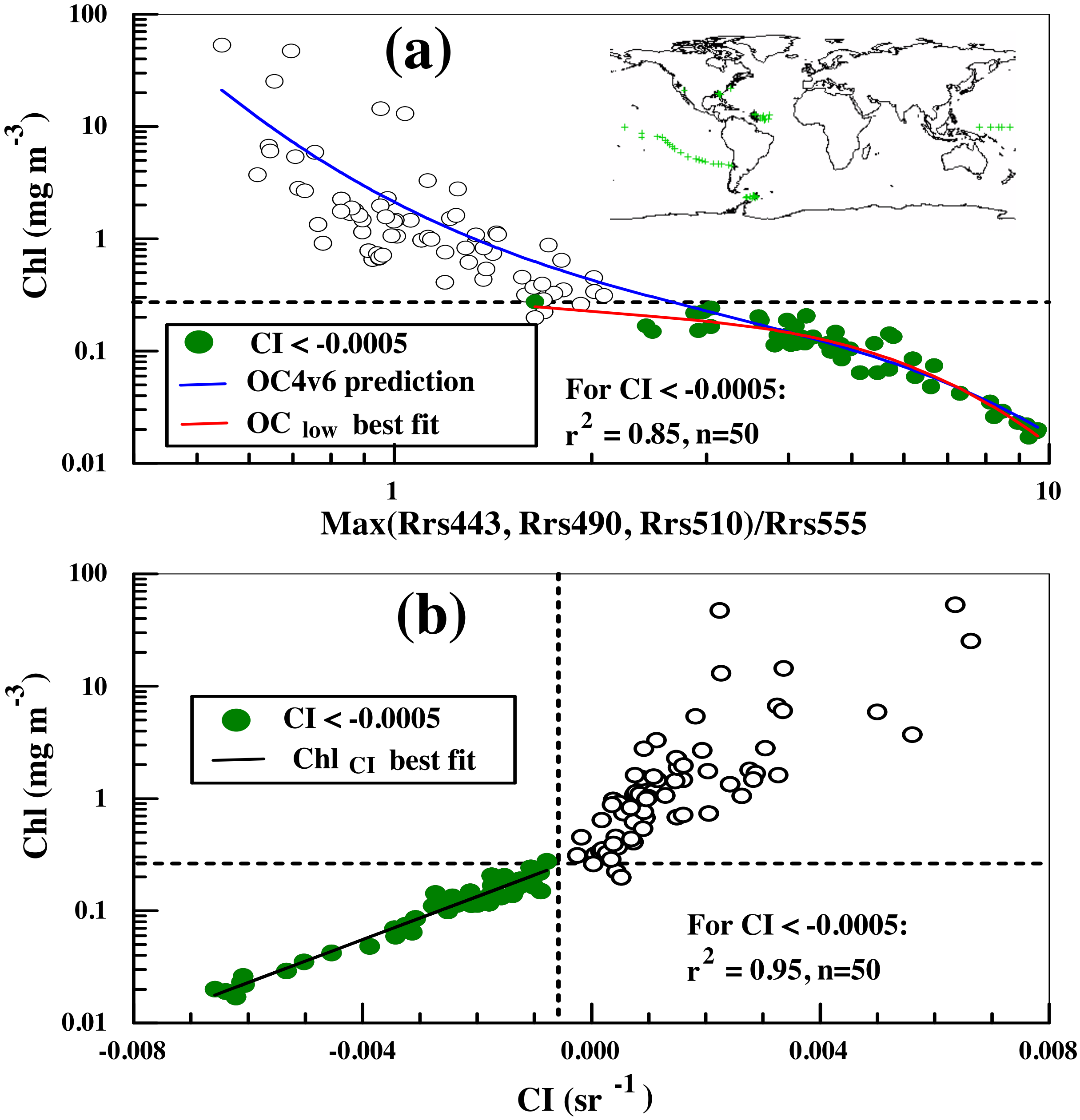

Fig. 3. Relationship between *in situ* chlorophyll-a concentration (Chl) and (a) reflectance ratio *R* and (b) color index (CI). The highlighted points emphasize those corresponding to CI ≤ -0.0005, where the corresponding data collection locations are shown in the inset map. Note that the minimum Chl in this dataset is about 0.02 mg m^{-3}. In (a), the RMS error is estimated between measured and OC4v6 predicted Chl. If a best fit from all data points for CI < -0.0005 sr^{-1} is used, RMS error is reduced to 22.95%. Statistics are presented in Table 1.

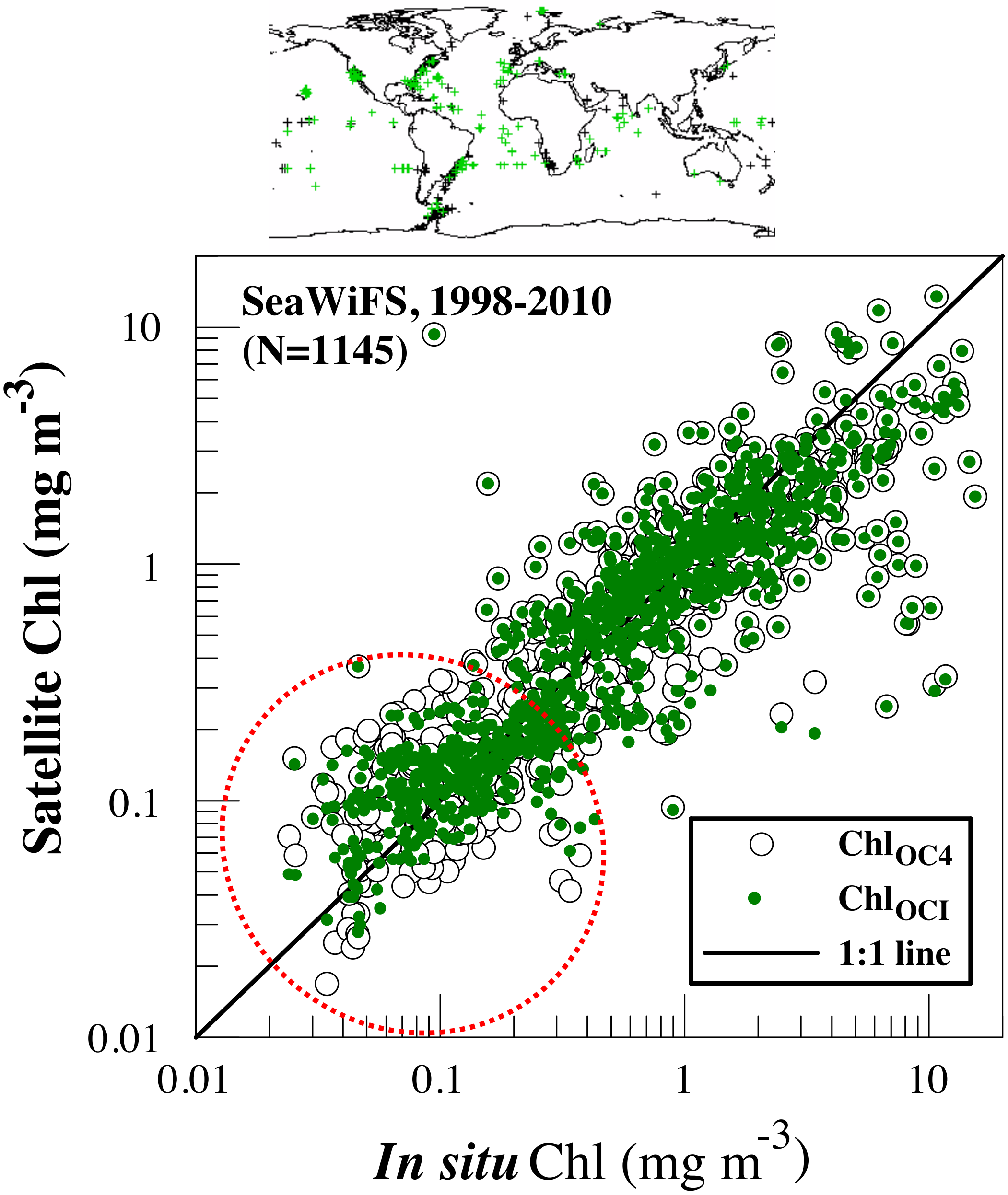

Fig. 4. Comparison between *in situ* Chl and satellite-based Chl for SeaWiFS. The satellite Chl was derived from both the OC4v6 algorithm (empty circles) and OCI algorithm (dots). Note that for Chl > 0.4 mg m^{-3} the results from the two algorithms were forced to be identical (Eq. 5). The locations of the *in situ* measurements for Chl ≤ 0.25 mg m^{-3} are shown in the corresponding map. The comparison statistics for low concentration (Chl ≤ 0.25) are listed in Table 2.

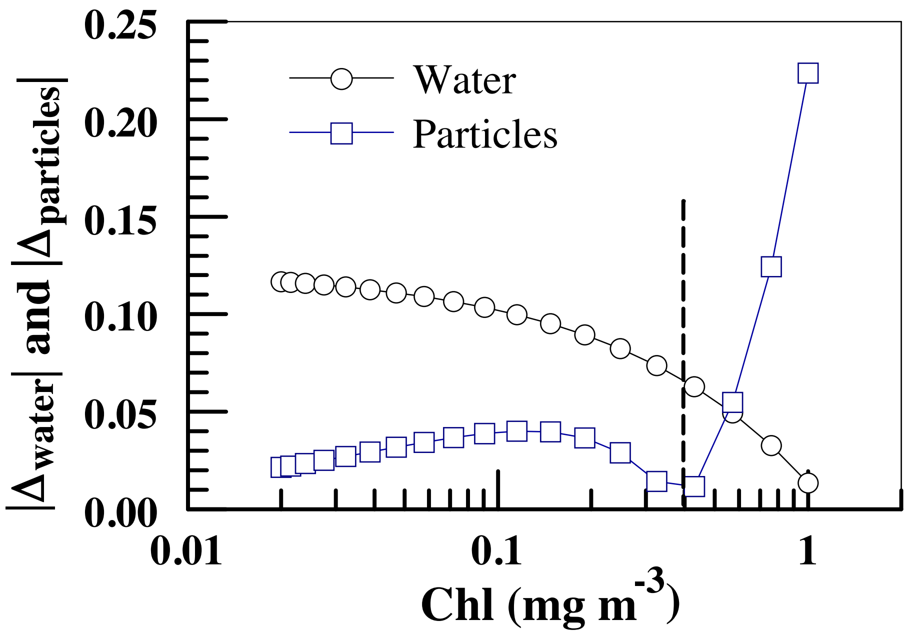

Fig. 5. Relationship between the two backscattering terms in Eq. (9) with Chl. To show their relative magnitudes, the absolute values (x 1000) are shown here. Note that for Chl ≤ 0.4 mg m^{-3}, the water term dominates the numerator of Eq. (9).

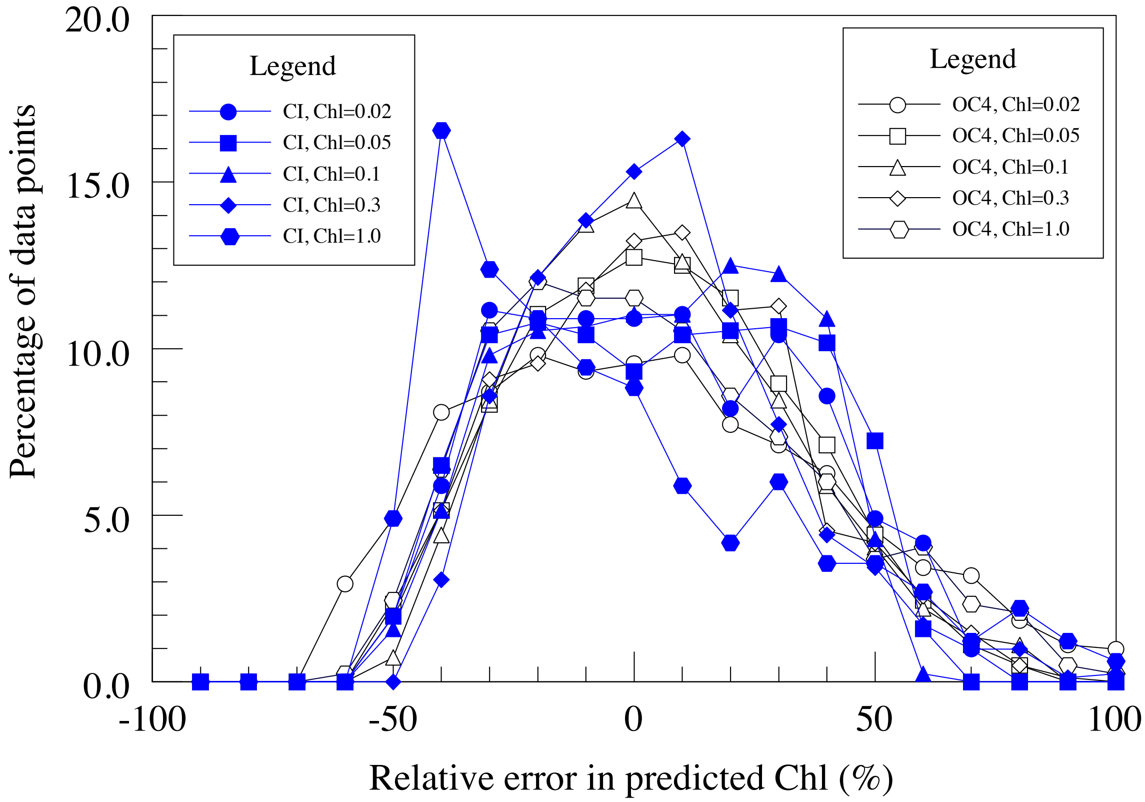

Fig. 6. Chl algorithm sensitivity to independent changes of detrital particles and CDOM relative to phytoplankton, based on 816 model simulations for each Chl value (Eq. 6, 13-15).

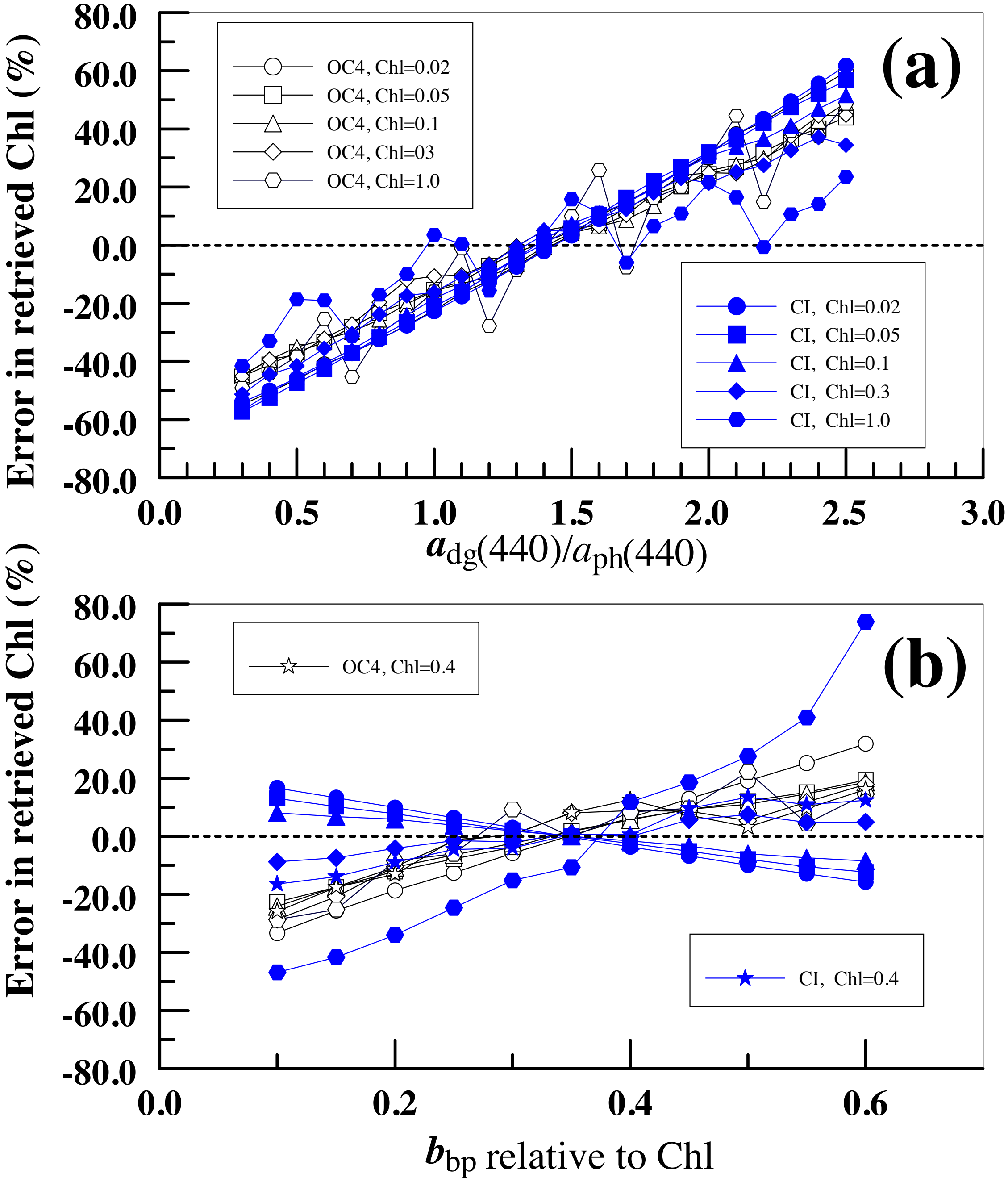

Fig. 7. Chl algorithm sensitivity to independent changes of absorption of detrital particles and CDOM (a_{dg}) relative to Chl (a), and to independent changes of particular backscattering (b_{bp}) relative to Chl (b), based on model simulations for each Chl value (Eq. 6, 13-15). Note that in (b), the added simulation was for Chl = 0.4 (star symbols), when the errors in the CI retrievals are shown to approach those of the OC4 retrievals.

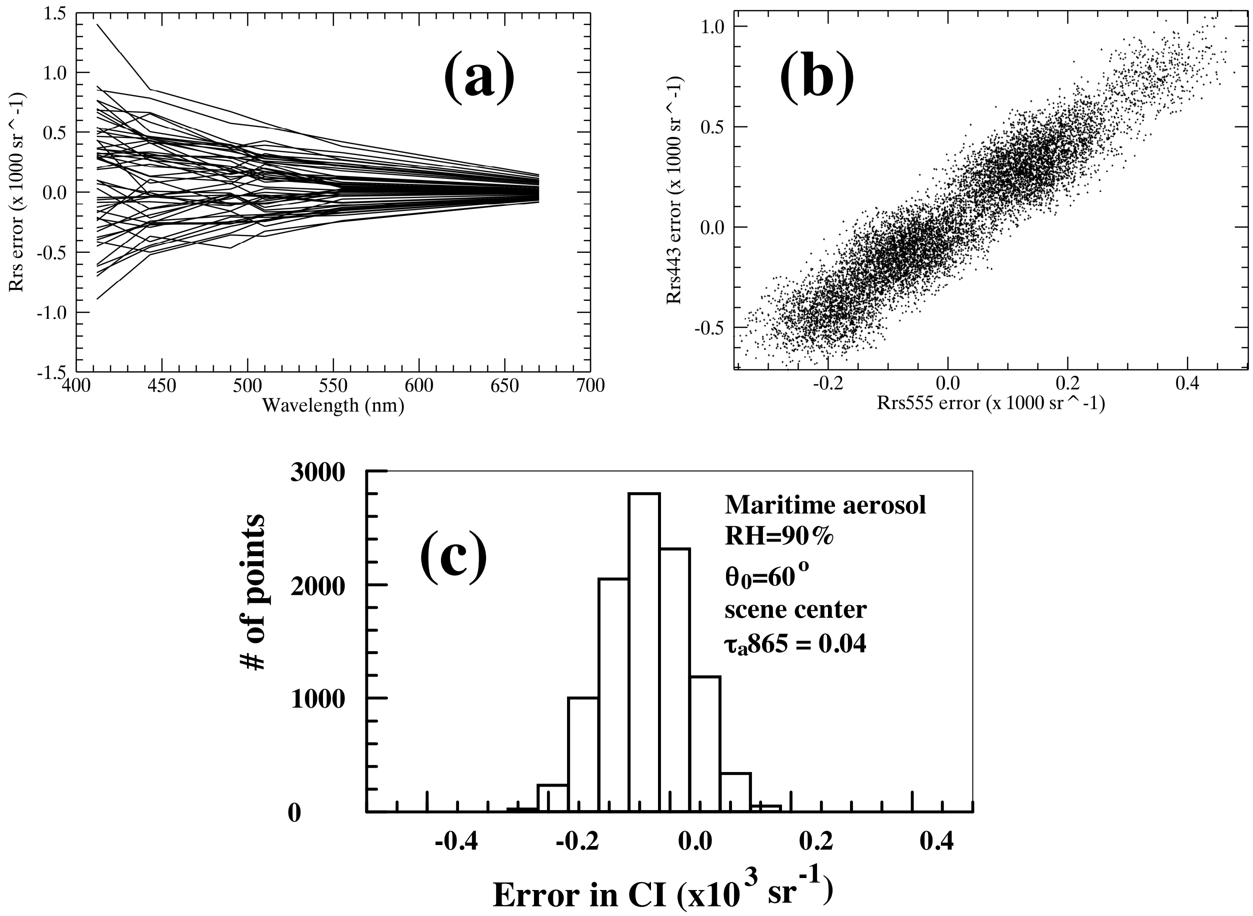

Fig. 8. Errors in $R_{rs}(\lambda)$ and CI induced by SeaWiFS digitization-noise after applying the Gordon and Wang (1994a) atmospheric correction. Most of the errors are due to the impact of the small noise on the atmospheric correction bands in the near infrared, which extrapolate the atmospheric properties to the visible (Hu et al., 2001). These errors are approximately linear to changing wavelengths (a and b), and can thus be corrected to first order by the CI algorithm (Eq. 3, Fig. 2), resulting in smaller errors in CI (and Chl_{CI}, see Fig. 9). The model parameters are listed in (c). Results from other modeling scenarios are different, but the principles in reducing the noise-reduced errors using the CI are the same.

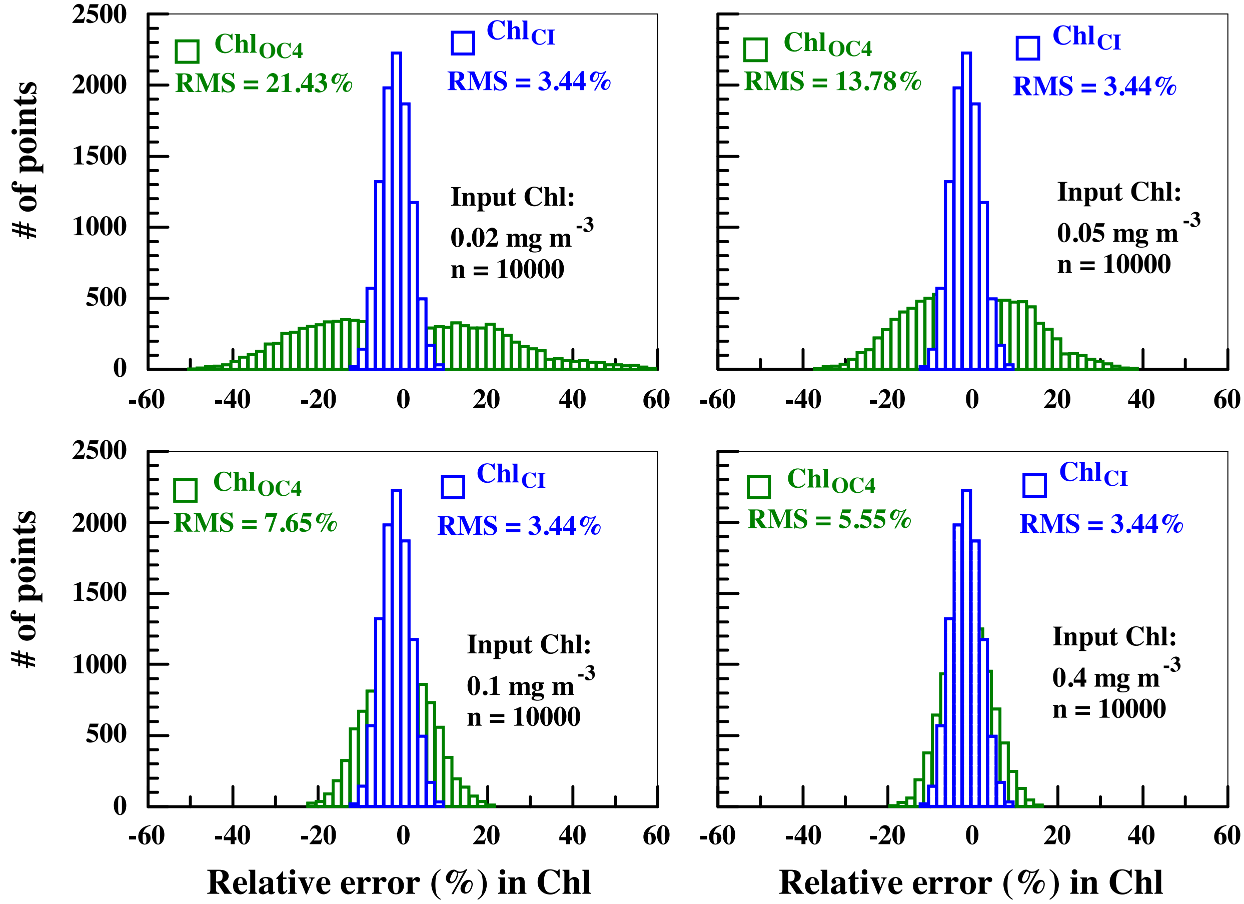

Fig. 9. Error distribution in the retrieved Chl due to digitization-noise induced $R_{rs}(\lambda)$ errors for a clear maritime atmosphere (Fig. 8). *In situ* R_{rs} data for the input Chl concentrations (from 0.02 to 0.4 mg m^{-3}) were combined with the $R_{rs}(\lambda)$ errors to estimate Chl, where the "true" Chl was determined from the input R_{rs} data free of errors. The differences were used to determine the relative retrieval errors. Note that the CI-based retrieval errors are independent of Chl concentrations.

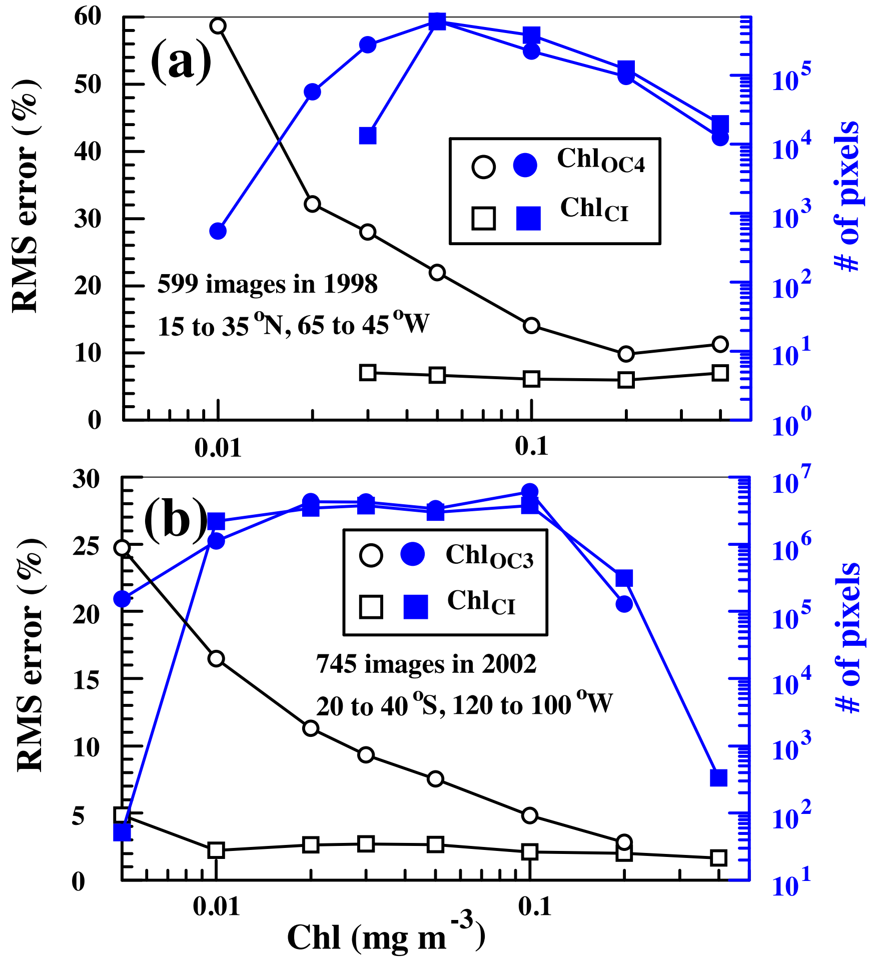

Fig. 10. (a) Statistics of speckling error in SeaWiFS GAC images in 1998 (n=599) for a 20 x 20^{o} region in the Sargasso Sea. The speckling error is defined as the relative difference between the original Level-2 Chl and a 3x3 median-filter smoothed Level-2 Chl, with the assumption that most noise-induced speckling errors are removed in the latter. Note that while the RMS errors in Chl$_{OC4}$ increase sharply with decreasing concentrations, RMS errors in Chl$_{CI}$ remain stable at a much lower level in the entire concentration range here. The overall patterns agree well with those from the model simulations (Fig. 9), suggesting that most of these speckling errors originate from digitization/noise (through atmospheric correction). The total number of valid pixels from each algorithm indicates that all Chl$_{OC4}$ ≤ 0.02 mg m^{-3} appear unrealistic due to primarily atmospheric correction artifacts. (b) Same as in (a), but data were extracted from MODIS/Aqua Level-2 images in 2002 (n=745) for a 20 x 20^{o} subregion in the Southern Pacific.

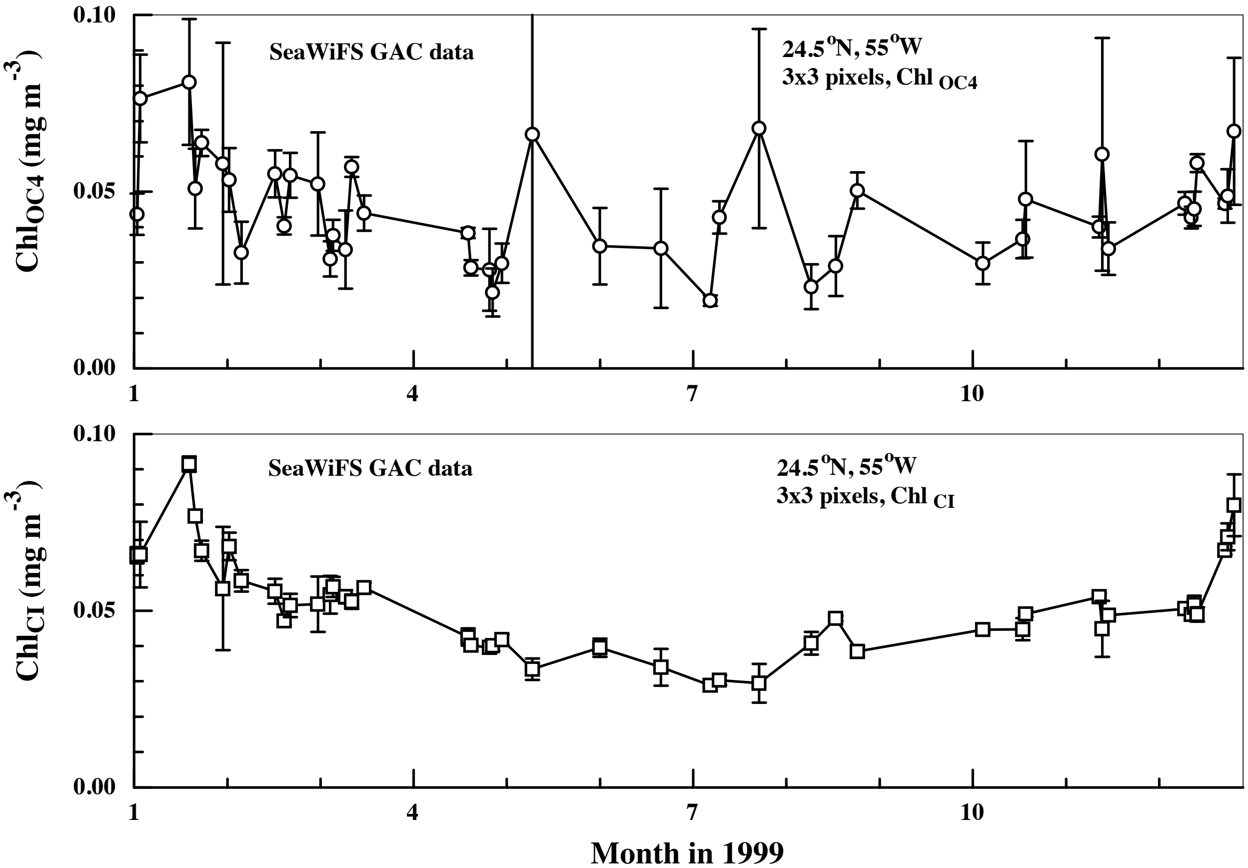

Fig. 11. Chl (mg m^{-3}) time series derived from SeaWiFS GAC $R_{rs}(\lambda)$ data using the OC4v6 algorithm (top) and the CI algorithm (bottom). Data were extracted from 3x3 pixels centered at 24.5°N 55°W from the daily measurements. For any given image (date), only when more than half of the pixels (in this case, ≥5 pixels) contained valid data (i.e., not associated with any suspicious flags) were statistics estimated.

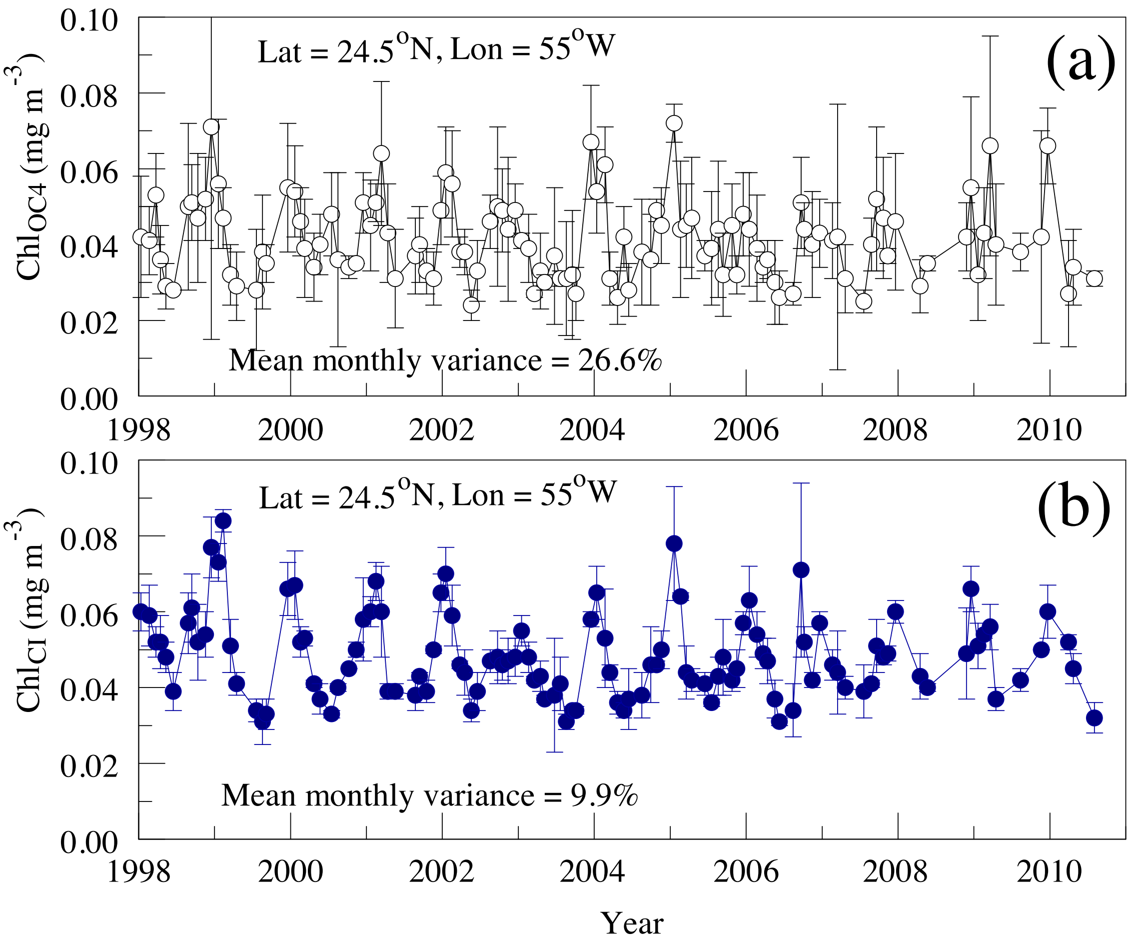

Fig. 12. Chl (mg m^{-3}) time series derived from SeaWiFS GAC $R_{rs}(\lambda)$ data using the OC4v6 algorithm (top) and the CI algorithm (bottom). Data were first extracted from 3x3 pixels centered at 24.5°N 55°W from the daily measurements. For any given image (date), only when more than half of the pixels (in this case, ≥5 pixels) contained valid data (i.e., not associated with any suspicious flags) were statistics estimated. The daily data were then averaged for the calendar month to construct the monthly time series. Note that SeaWiFS was not continuously operational after 2005 due to instrument operations.

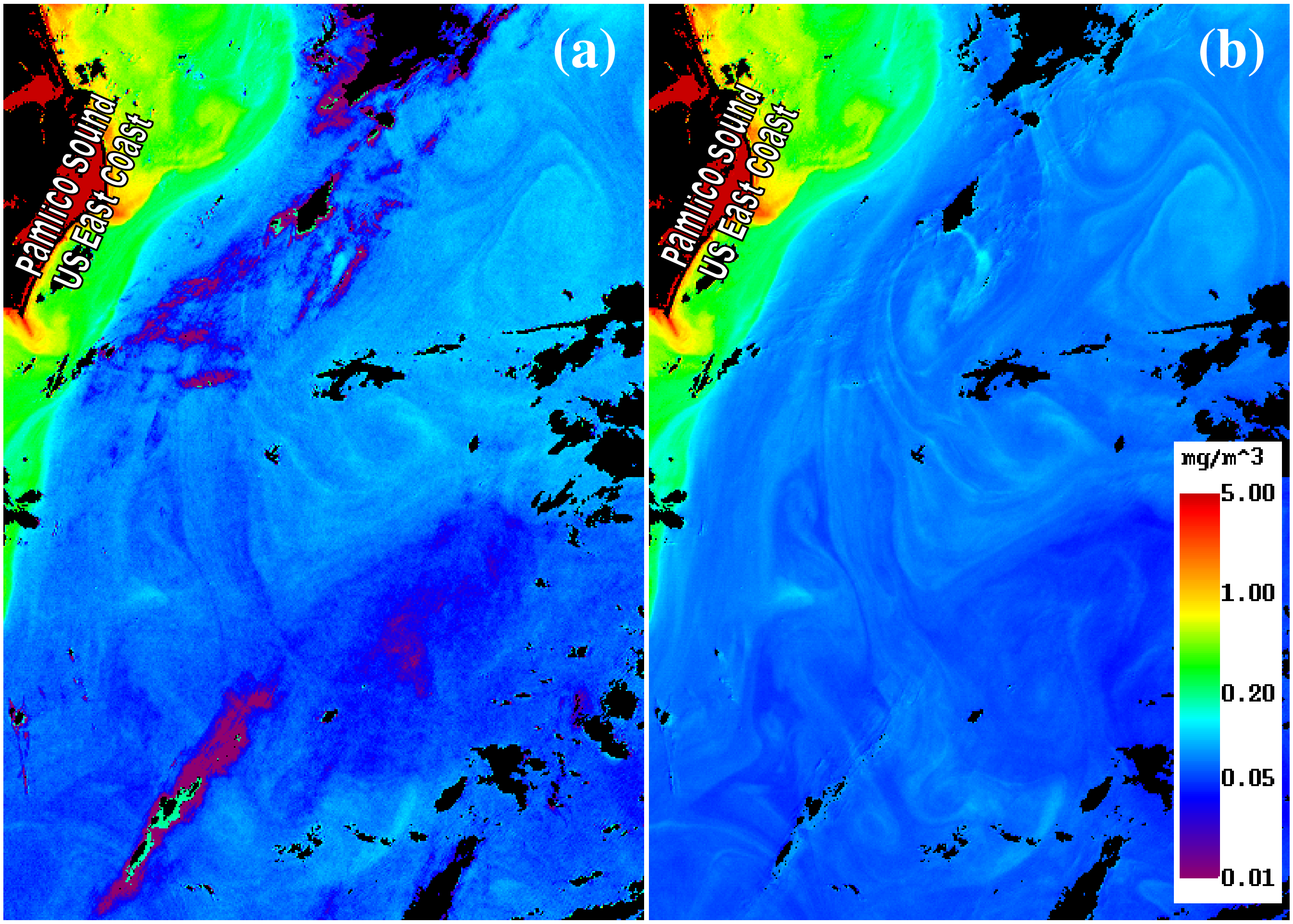

Fig. 13. Comparison between SeaWiFS Level-2 Chl_{OC4} (a) and Chl_{OCI} (b) over the western North Atlantic Ocean. SeaWiFS data were collected on 1 June 2004 (17:15 GMT) and processed with SeaDAS6.1. The Level-2 quality-control flags were turned off to show the circulation features. Note that some eddy features are clearly revealed in the Chl_{OCI} image but absent in the Chl_{OC4} image due to noise and residual errors in atmospheric correction and other corrections.

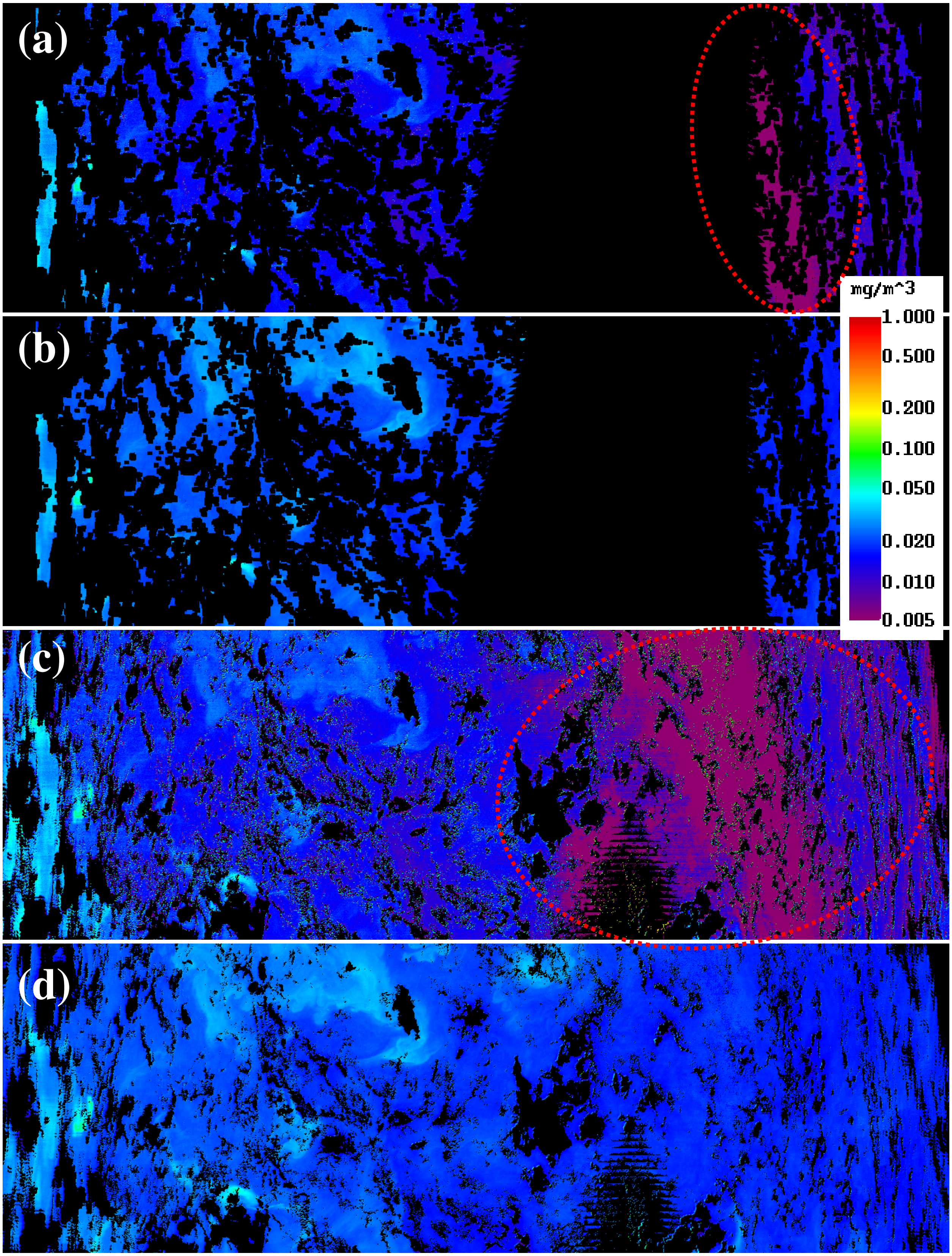

Fig. 14. MODIS/Aqua Level 2 Chl_{OC3} and Chl_{OCI} derived from a subregion in the South Pacific Gyre (about 2200 x 440 km centered at 25.2°S 110.8°W) on 4 March 2003, 21:10 GMT. (a) and (c) show the default Chl_{OC3} when the quality control flags are on and off, respectively. (b) and (d) are the corresponding Chl_{OCI} images.

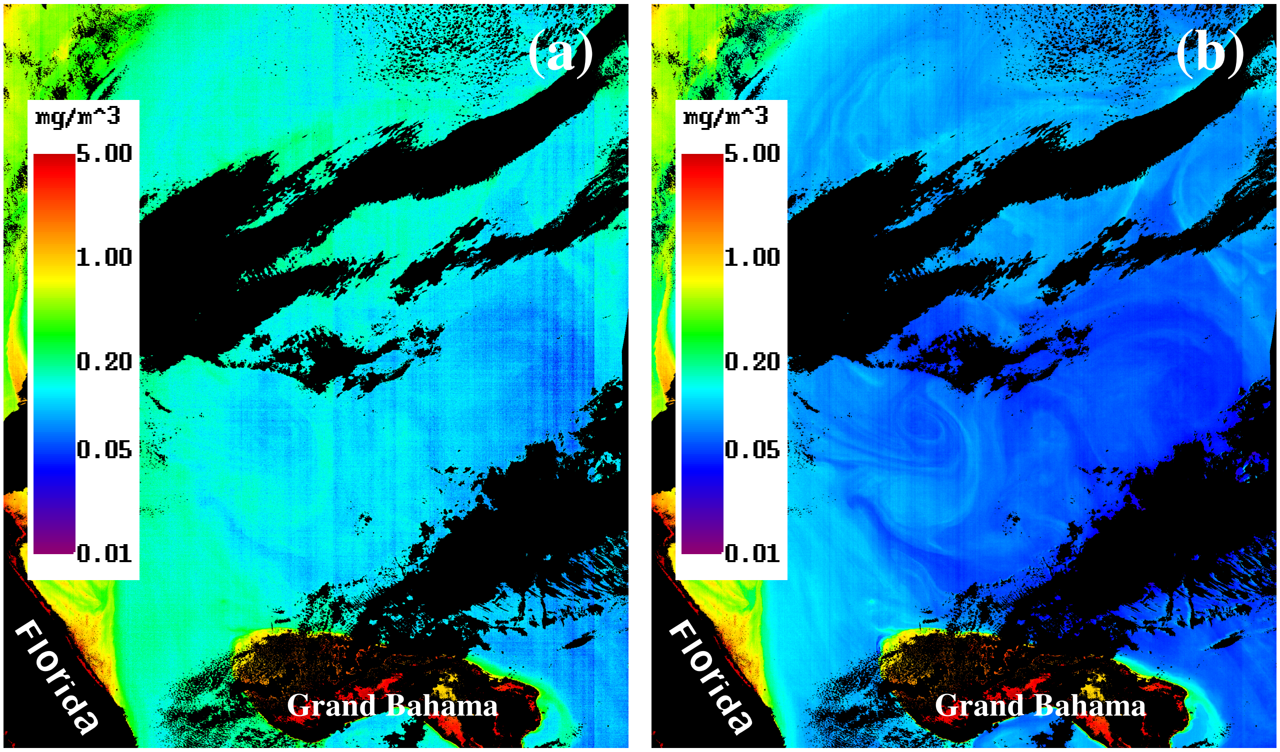

Fig. 15. Comparison between MERIS full-resolution (FR) Chl_{OC3} (a) and Chl_{OCI} (b) over the western North Atlantic Ocean. MERIS data were collected on 7 May 2011 (15:21 GMT) and processed with SeaDAS6.1. Note that most speckling and vertical striping noise in the Chl_{OC3} image has been removed in the Chl_{OCI} image, where several eddy and circulation features can be better observed. Further, although the same algorithm coefficients for SeaWiFS were used, Chl_{OCI} values in offshore water appear to be closer than Chl_{OC3} to those from SeaWiFS for the same region during similar periods (Fig. 13).

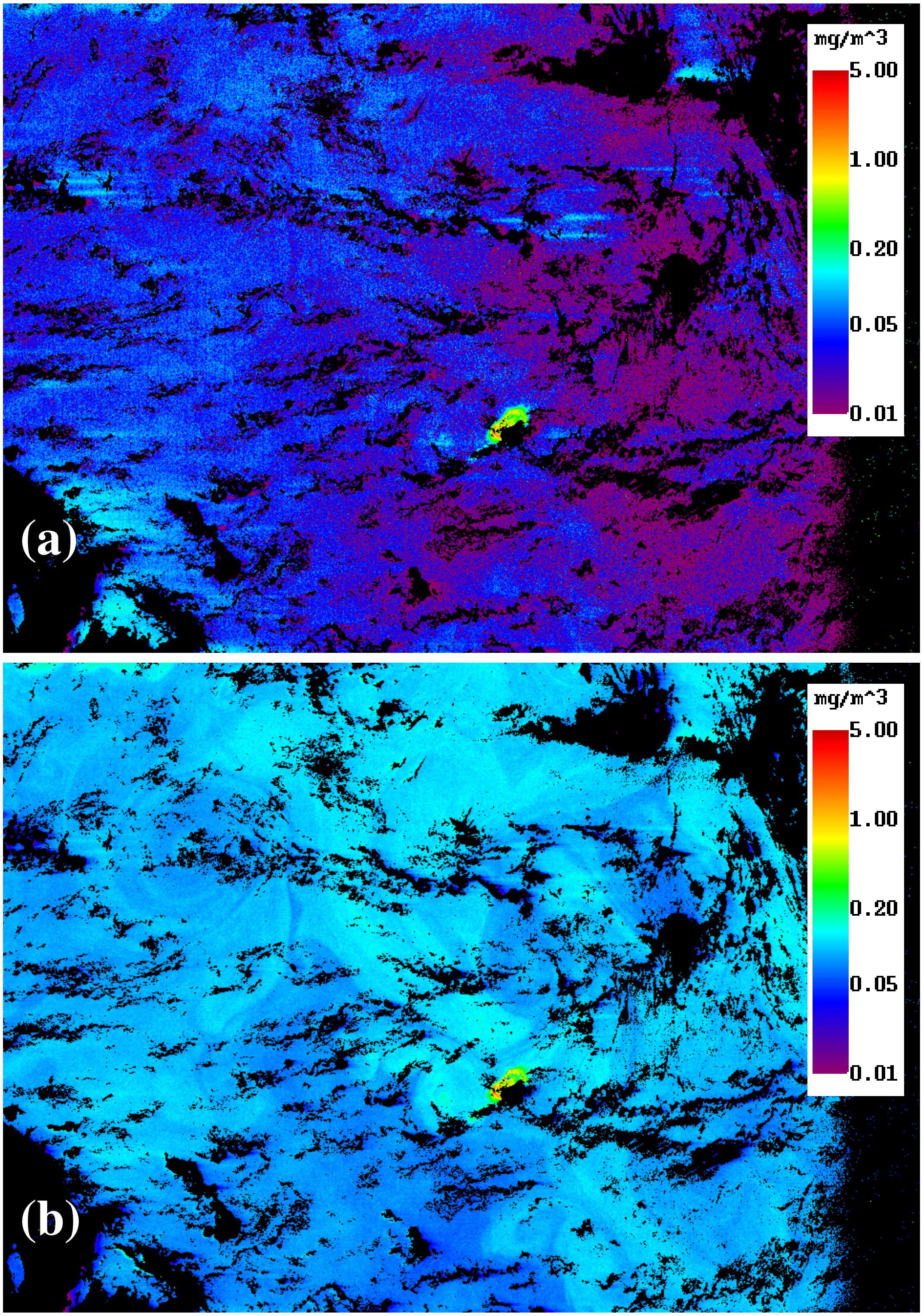

Fig. 16. Comparison between CZCS Level-2 Chl_{OC2} (a) and Chl_{OCI} (b) over the western North Atlantic Ocean (about 30^o – 36^{o}N, 70^o – 60^{o}W). CZCS data were collected on 31 July 1983 (16:02 GMT) and processed with SeaDAS6.1. Note that all eddy and circulation features in the Chl_{OCI} image are completely absent in the Chl_{OC2} image.

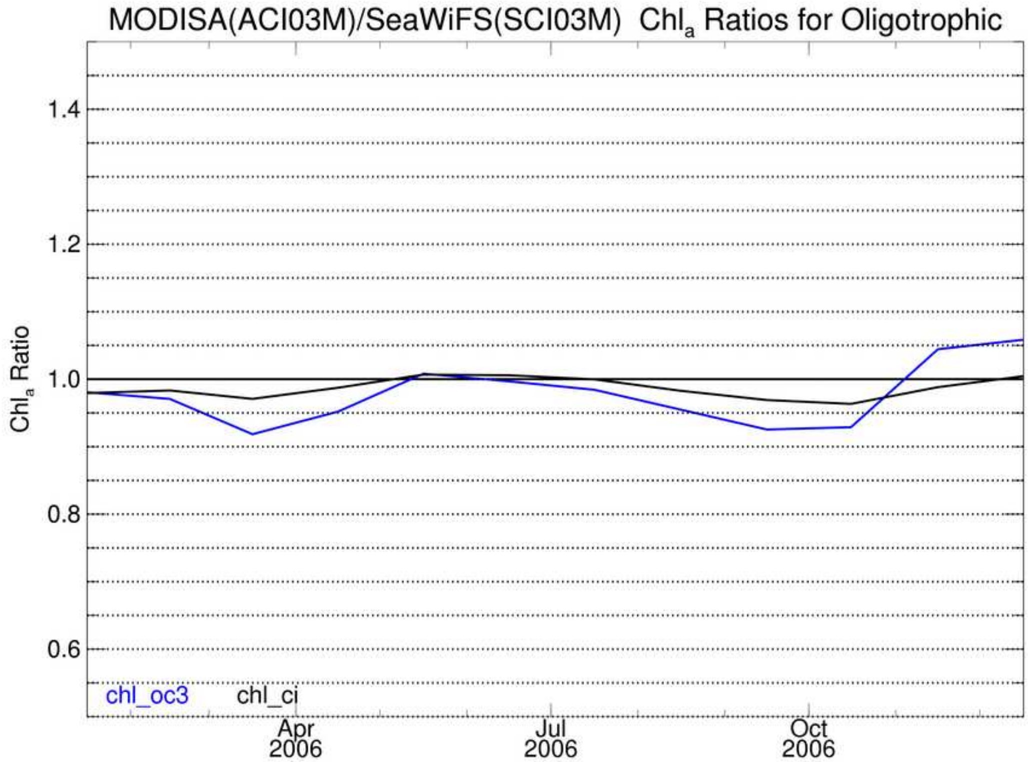

Fig. 17. Mean Chl ratio over global oligotrophic oceans between MODIS/Aqua and SeaWiFS estimates using the OCx (blue) and CI (black) algorithms. Here "oligotrophic" is defined as all 9-km pixels with SeaWiFS mission mean Chl ≤ 0.1 mg m^{-3}.

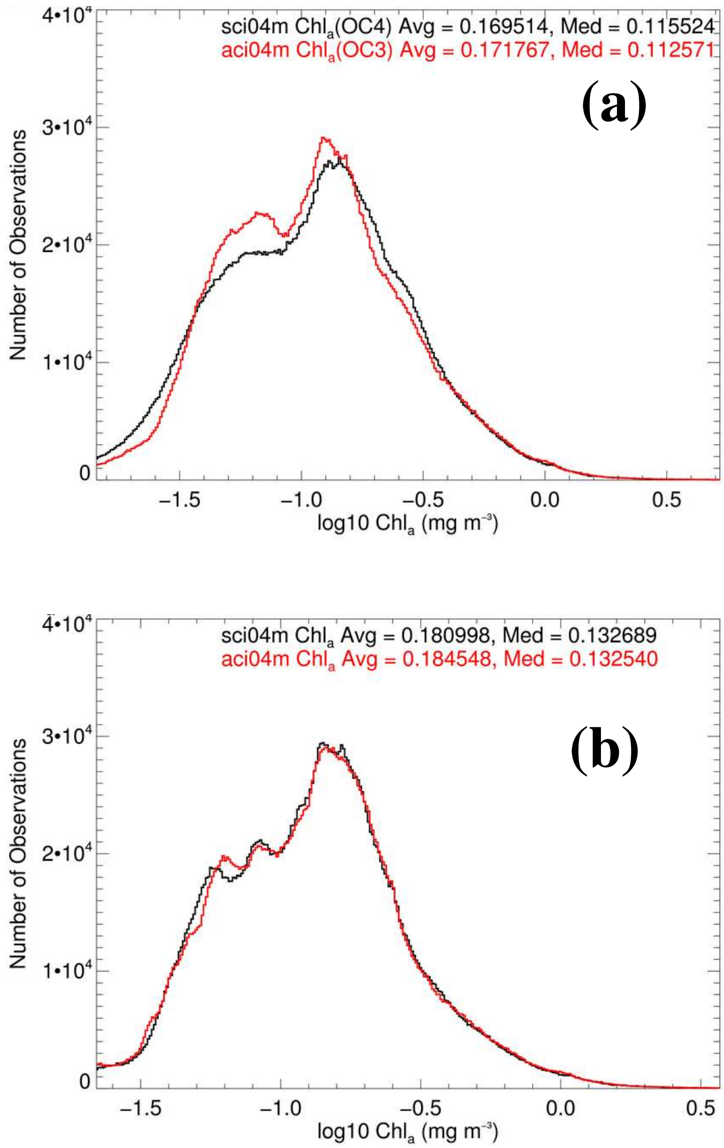

Fig. 18. Chl distribution in the global deep oceans (> 200 m) during November 2006, as derived from SeaWiFS (black) and MODIS/Aqua (red) measurements. Results in (a) are from the OCx band-ratio algorithms, and in (b) are from the CI algorithm (blended with the OCx algorithms for Chl > 0.25 mg m^{-3}). Note the offset of 0.01 – 0.02 mg m^{-3} in the global mean and median values between (a) and (b). Results from other months of 2006 show similar improvements in histogram consistency.